Chemical Geology 670 (2024) 122412

Contents lists available at ScienceDirect

Chemical Geology

journal homepage: www.elsevier.com/locate/chemgeo

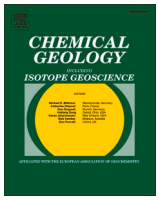

Mesoproterozoic depleted spinel peridotites metasomatized by high-K hydrous melt in the Patagonian back-arc

Aline Alves dos Santos [a], Tiago Jalowitzki [a,*], Fernanda Gervasoni [b,c], Maurizio Mazzucchelli [d], Tommaso Giovanardi [d], Manuel Enrique Schilling [e], Maria Isabel Varas-Reus [f], Yuji Orihashi [g], Rodrigo Freitas Rodrigues [h], Richard Walter Carlson [i], Georgina Marianela Rubiano Lorenzoni [j,k], Daiji Hirata [l], Gustavo Walter Bertotto [j]

[a] Universidade de Brasília, Instituto de Geociências, Programa de Pós-graduação em Geologia, Brazil
[b] Centro de Engenharias, Universidade Federal de Pelotas (UFPel), Brazil
[c] Programa de Pós-graduação em Geociências, Universidade de Federal do Rio Grande do Sul (UFRGS), Brazil
[d] Dipartimento di Scienze Chimiche e Geologiche, Universitá di Modena e Reggio Emilia, Italy
[e] Instituto de Ciencias de la Tierra, Facultad de Ciencias, Universidad Austral de Chile, Chile
[f] Department of Geosciences, University of Tuebingen, Germany
[g] Department of Earth and Environmental Sciences, Hirosaki University, Japan
[h] Research School of Earth Science, Australian National University (ANU), Australia
[i] Earth and Planets Laboratory, Carnegie Institution for Science, Washington, DC, United States of America
[j] INCITAP, CONICET - Universidad Nacional de La Pampa, La Pampa, Argentina
[k] Estelar Resources LTD S.A, Pan American Silver, Yacimiento Cerro Moro, Santa Cruz, Argentina
[l] Kanagawa Prefectural Museum of Natural History, Japan

ARTICLE INFO

Editor: Dr. S Aulbach

Keywords:
Spinel peridotites
Partial melting
Mesoproterozoic
Hydrous and high-K mantle metasomatism
Os isotopes
Patagonian mantle

ABSTRACT

Here we report the first investigation of spinel-bearing mantle xenoliths from Los Gemelos volcano, Canquel Plateau, Patagonia. They are highly-depleted Mesoproterozoic (*Re*—Os model ages of 1.3–0.9 Ga) harzburgites and clinopyroxene-poor lherzolites characterized by typical indicators of partial melt extraction, such as low whole-rock Al_2O_3 and CaO contents (<1.5 wt%), high Mg# of silicate phases (90–95), and Cr-rich spinel (Cr# 0.20–0.42). Depletion of incompatible highly siderophile elements (Re, Ru, Pd) relative to the primitive upper mantle supports high degrees of melt extraction. The occurrence of phlogopite and K-rich alkaline glass veins with high- and low-SiO_2 compositions is clear evidence of modal metasomatism. The light rare earth element (LREE) enrichment in clinopyroxene, as well as the whole-rock U-shaped REE pattern, confirms cryptic metasomatism. This melt-rock interaction is corroborated by major (i.e., Mg# vs. basaltic elements) and trace (i.e., La/Yb_N vs. Sr/Y and Ti/Eu; and Sr vs. Ti/Eu) element contents of pyroxenes. The calculated compositions of melts in equilibrium with clinopyroxene coexisting with phlogopite suggest interaction with slab-derived materials. This metasomatism has been generated by a chromatographic fractionation-reaction process, from deep to shallow mantle domains. The percolation of a high-K hydrous magma probably is associated with the upwelling of asthenospheric material through a slab-window, which caused partial melting of oceanic crust and overlying sediments during the Paleocene. The varying intensities of metasomatic imprints recorded by mantle xenoliths from Los Gemelos provide valuable insights into the interaction of slab-derived materials near the lithosphere-asthenosphere boundary, at a distance of ~600 km from the Andean volcanic arc.

1. Introduction

Several subduction-related components, such as oceanic crust (generating silicate or CO_2-rich melts), sediments, and seawater have a strong influence on the complex tectonic evolution recorded by the chemically and lithologically heterogeneous subcontinental lithospheric mantle (SCLM) beneath Patagonia (Stern et al., 1999; Gorring and Kay, 2000; Laurora et al., 2001; Kilian and Stern, 2002; Rivalenti et al., 2004,

* Corresponding author.
E-mail address: jalowitzki@unb.br (T. Jalowitzki).

https://doi.org/10.1016/j.chemgeo.2024.122412
Received 18 February 2024; Received in revised form 12 September 2024; Accepted 13 September 2024
Available online 16 September 2024

2007; Bjerg et al., 2005, 2009; Ntaflos et al., 2007; Schilling et al., 2008, 2017; Dantas et al., 2009; Faccini et al., 2013; Mundl et al., 2015, 2016; Jalowitzki et al., 2016, 2017; Melchiorre et al., 2020; Bertotto et al., 2021, 2022; Novais-Rodrigues et al., 2021). Notably, severe lithospheric thinning has been triggered beneath Central-North Patagonia (~43–45°S) since ~300 Ma (Jalowitzki et al., 2024). In this context, mantle xenoliths from Los Gemelos, located on the northern edge of the Deseado Massif, represent fragments from near the lithosphere-asthenosphere boundary (LAB) (Jalowitzki et al., 2024).

Mantle metasomatism beneath Patagonia has been mainly associated with recycling of materials derived from the Andean subduction system along the western margin of South America during the Phanerozoic. Interactions between peridotite and melts/fluids derived from subducted slabs can produce modal metasomatism in the form of mica (phlogopite) and/or amphibole (pargasite) (e.g., Wyllie and Sekine, 1982; Canil and Scarfe, 1989; Stern et al., 1999; Gorring and Kay, 2000; Laurora et al., 2001; Grégoire et al., 2002; Neumann et al., 2004; Arai and Ishimaru, 2008; Giuliani et al., 2016; Jalowitzki et al., 2016; Aulbach et al., 2017, 2020; Kargin et al., 2019; Bonadiman et al., 2021). Moreover, glass veins with variable compositions are also evidence of mantle metasomatism (e.g., Kepezhinskas et al., 1995; Neumann and Wulff-Pedersen, 1997; Yaxley et al., 1997; Rapp et al., 1999; Grégoire et al., 2001; Laurora et al., 2001; Franz et al., 2002; Arai et al., 2003; Kilian and Stern, 2002; Gervasoni et al., 2017; Corgne et al., 2018). These indicators of modal metasomatism are normally associated with the chemical enrichment of the coexisting primary mineral phases, being characterized by high incompatible over less incompatible element ratios (i.e., light rare earth elements - LREE over heavy rare earth elements - HREE).

Aiming to constrain the origin and time of depletion and metasomatic events recorded in the SCLM beneath the northern edge of the Deseado Massif, we evaluate the influence of a Paleocene (~60 Ma) slab-window as a potential heat source to cause partial melting of the adjacent oceanic crust and overlying sediments. We show that the melt-rock interaction caused crystallization of phlogopite and chemical enrichment of whole-rock and clinopyroxene from the mantle section underneath Los Gemelos. The identification of phlogopite-bearing mantle xenoliths contributes to a better understanding of asthenosphere-lithosphere interaction involving melt/fluid migration into the mantle wedge. Due to the lack of reaction zones between K-rich alkaline glass veins and peridotite, we conclude that these veins represent an analogue to proto-kimberlite metasomatism (e.g., Giuliani et al., 2014, 2016; Aulbach et al., 2017; Tappe et al., 2018; Kargin et al., 2019; Gervasoni et al., 2022; Rodrigues et al., 2023; Braga et al., 2024), occurring immediately before, or coeval with, the ascent of the host magma. In addition, *Re*—Os model ages (T_{RD} and T_{MA} = 1.3–0.9 Ga) reinforce a common origin for the SCLM beneath Patagonia, Malvinas/Falkland Islands, and southern South Africa (Schilling et al., 2008, 2017; Mundl et al., 2015, 2016). Therefore, these mantle-derived xenoliths provide a valuable opportunity to investigate the tectono-magmatic processes involved in the long-lived and complex evolution of the Patagonian back-arc. In this study, we present mineral and whole-rock geochemistry, Os isotopic composition, and highly siderophile element abundances (HSE; platinum group elements - PGEs + Re) for 16 spinel-bearing xenoliths.

2. Geological setting

The Canquel Plateau represents the southern extension of the Somuncura large igneous province (Anselmi et al., 2004; Massaferro et al., 2017) (Fig. 1). Pleistocene Los Gemelos volcano (0.54–0.34 Ma; Table S1) hosts the mantle xenoliths investigated here and outcrops in the inferred collision zone developed during the Carboniferous-Permian between the Deseado and the North Patagonian massifs (Pankhurst et al., 2006; Schilling et al., 2017; Jalowitzki et al., 2024). The basement ages of these two massifs suggest the occurrence of two main episodes of crust formation. The oldest event is evidenced by rocks with Paleo- to Mesoproterozoic model ages and detrital zircon populations related to Rodinia consolidation (1.3–0.9 Ga), whereas the youngest rocks have Pampean and Brasiliano ages related to Rodinia fragmentation and to the early stages of Gondwana consolidation (0.75–0.55 Ga) (Pankhurst and Rapela, 1995; Hervé et al., 2003; Pankhurst et al., 2003, 2006, 2014; Ramos, 2010; Martínez Dopico et al., 2011; Schilling et al., 2017). Therefore, Patagonia was part of the Rodinia supercontinent during the Mesoproterozoic, becoming detached during its break-up and, in the Neoproterozoic, being accreted to Gondwana (Ramos, 2010).

In the Cenozoic, slab-windows opened in the west margin of Patagonia, acting as potential mechanisms to metasomatize the SCLM (e.g., Cande and Leslie, 1986; Breitsprecher and Thorkelson, 2009; Jalowitzki et al., 2017). During the Paleocene to Eocene, the Farallon-Aluk spreading ridge collided against the South American continental plate. The triple junction formed through their intersection with the oceanic trench migrated southward along the western margin of South America. To the south, the continuous subduction of the Chile Ridge spreading center has been migrating from the southern edge of Patagonia to the latitude of the Taitao Peninsula (~46°S), forming a trench-ridge-trench triple junction for the last 16 Ma (e.g., Cande and Leslie, 1986; Breitsprecher and Thorkelson, 2009).

3. Analytical methods

In this study, we selected 16 mantle xenoliths large enough for geochemical and isotopic analysis that were also examined in thin sections. Modal proportions of mineral phases were determined by point-counting using the JMicroVision software (Roduit, 2007). For each thin section (24 × 40 mm), between 2034 and 3826 points were counted. The rock fragments were firstly disaggregated by the SELFRAG™ Lab system at the University de Brasília (UnB). Subsequently, any weathered crystals were removed from the disaggregated sample by careful handpicking under a binocular microscope. Mineral major element analyses were determined in the 16 selected samples (Table S2), whereas mineral trace and rare earth element (REE) abundances were obtained in a subset of 10 representative samples (Table S3). All sample aliquots (obtained after SELFRAG™ separation and removal of weathered minerals) were finely ground into powder using an agate mortar and were analyzed for their whole-rock major and trace element compositions (n = 9, Table S4), and Os isotopic compositions and HSE abundances (n = 6) (Table S5). The whole-rock geochemistry and K—Ar age of three representative volcanic rocks hosting the mantle xenoliths from Los Gemelos were determined (Table S1). Considering the importance of the mineral chemistry, *Re*—Os, and highly siderophile elements to our discussion, they are presented below. The remaining analytical methods are detailed in the Supplementary Information and the reference materials are presented in Tables S6 and S7.

3.1. Electron probe microanalysis

Major element concentrations of mineral phases (olivine, orthopyroxene, clinopyroxene, spinel, and phlogopite) and glass veins from Los Gemelos mantle xenoliths were determined by wavelength-dispersive spectrometry (WDS) using a JEOL JXA-8230 Electron Probe Micro Analyzer (EPMA) at the Laboratório de Microssonda Eletrônica, Instituto de Geociências (IG), UnB, Brazil. The analyses were done using an accelerating voltage of 15 kV, a beam current of 10 nA, and a beam diameter of 1 μm in the spot mode. For phlogopite measurements, we employed the circle mode with 5 μm diameter. Counting times on peak were 10 s per analyte peak and 5 s for the background. All results were reduced using an in-house ZAF correction program. The measurements were calibrated with the following mineral standards: andradite (CaO and FeO), albite (Na_2O), forsterite (MgO), microcline (K_2O, Al_2O_3 and SiO_2), pyrophanite (TiO_2 and MnO), chromium oxide (Cr_2O_3), nickel oxide (NiO), topaz (F), and vanadinite (V_2O_3 and Cl). The detection

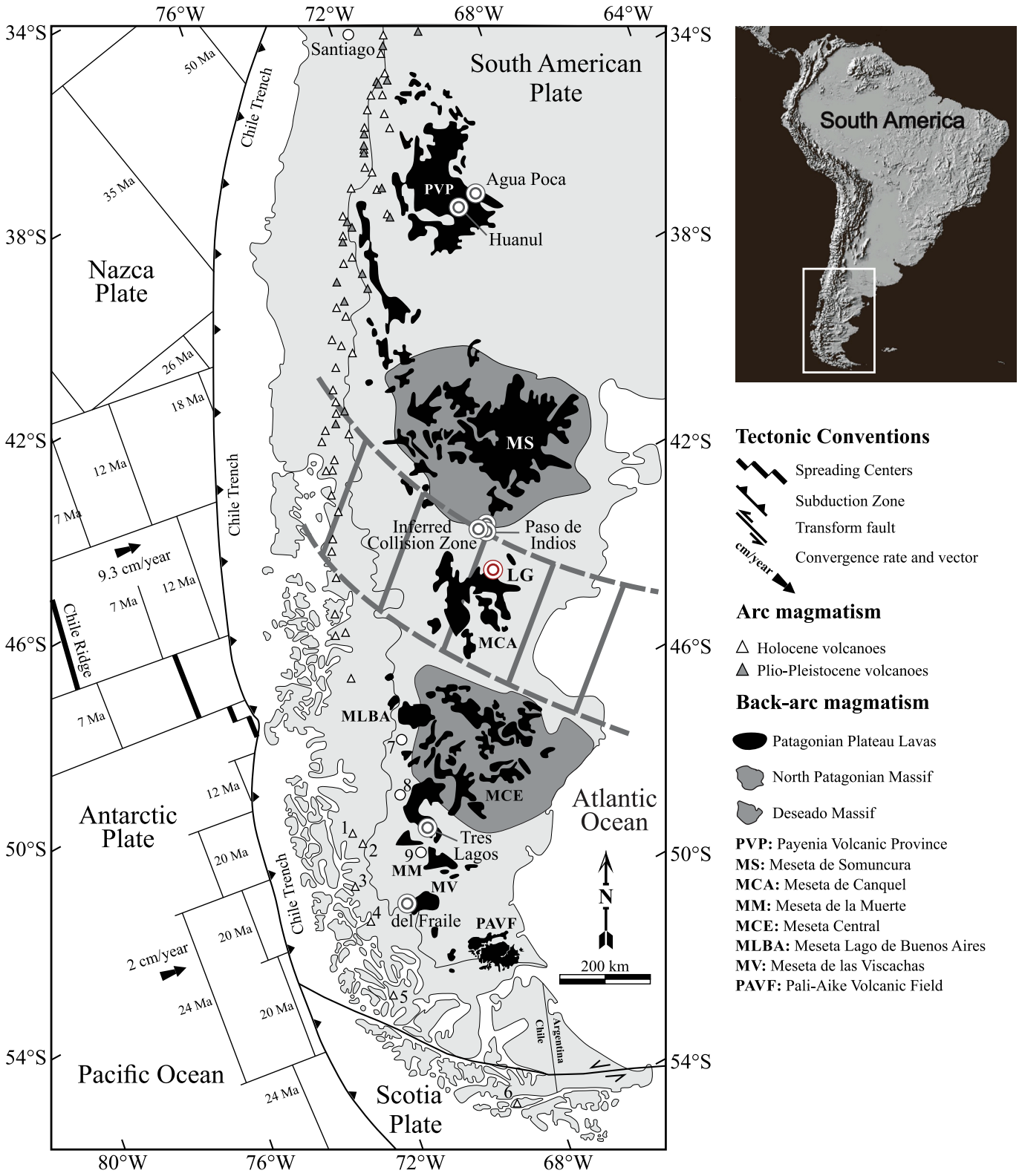

Fig. 1. Map of southern South America showing the location of the Los Gemelos volcano (LG). Depleted mantle xenoliths are from Agua Poca, Huanul, and Tres Lagos while adakite metasomatized xenolith samples are from Paso de Indios region (Chenque, Matilde, and León) and Cerro del Fraile. The occurrence of adakite lavas in the Austral Volcanic Zone (AVZ) is indicated as 1 = Lautaro, 2 = Viedma, 3 = Aguilera, 4 = Reclus, 5 = Mt. Burney, 6 = Cook Island, whereas in the back-arc region of Southern Volcanic Zone is 7 = Cerro Pampa, 8 = Chaitén, and 9 = Puesto Nuevo.

limits for all analyzed mineral phases are indicated in Table S2.

3.2. Laser ablation inductively coupled plasma mass spectrometry

Clinopyroxene and phlogopite trace element abundances were determined at the laboratory of the Centro Interdipartimentale Grandi Strumenti (CIGS), the Università di Modena e Reggio Emilia, Italy. A Thermo Fisher Scientific XSERIES-2 mass spectrometer coupled to a New Wave UP 213 laser ablation was used. Data reduction was performed with the Thermo Fisher Scientific PlasmaLab® software using NIST610 (Jochum et al., 2005) and BCR-2 basaltic glass (Jochum et al., 2015) as external standards (Table S7). The typical precision (BCR-2 < 10 %, except for W), accuracy (BCR-2 usually <20 %), and detection limits for all analyzed mineral phases are indicated in Table S7. The analysis conditions were laser spot 55 μm, output 70 % wt., Rep. Rate 10 Hz, dwell time 30 s and laser beam fluency at 8 J/cm^2. The sample surface was first ablated with 65 μm spot size, 45 % wt., 10 Hz repetition rate. The isotope ^{44}Ca was used as internal standard for clinopyroxene, whereas ^{29}Si was used for phlogopite. ThO/Th ratio was monitored on the NIST standard and set lower than 1 % during tuning. The Ba/Eu ratio in phlogopite was commonly higher than 5000, suggesting strong BaO interference on Eu. For this reason, the primitive mantle (PM, Sun and McDonough, 1989) normalized Eu (interpolated value) for phlogopite was calculated based on the adjacent REE elements using the square root of ($Sm_N \times Gd_N$, where N = PM normalized values), following the geometric method suggested by Taylor and McLennan (1985).

3.3. Re—Os and highly siderophile elements

Re—Os isotopic compositions and HSE contents were performed by the isotope dilution method at the Earth and Planets Laboratory (EPL), Carnegie Institution for Science, United States of America. Whole-rock powder (1 g) was digested using 6 ml of reverse aqua regia (2:1 HNO_3-HCl) at high-temperature (~240 °C) in Pyrex Carius tubes over a period of 24–72 h (Shirey and Walker, 1995), together with mixed spikes of ^{185}Re—^{190}Os and ^{191}Ir-^{99}Ru-^{194}Pt-^{105}Pd. Osmium was separated by solvent extraction employing high-purity CCl_4 and microdistillation in HBr following established techniques (e.g., Reisberg and Meisel, 2002). Rhenium, Ir, Pt and Pd were separated via anion exchange chromatography using AG1X8 resin. Osmium isotopic compositions were determined by negative thermal ionization mass spectrometry (N-TIMS) using the Thermo-Fisher Triton. Osmium was analyzed as OsO_3^- by single-collector peak-hopping in the electron multiplier. Measurements of the EPL J-M Os standard (former DTM standard) using this procedure during this study gave an average value of ^{187}Os/^{188}Os = 0.17395 ± 7 (2SD). This value is within error of the mean of high-precision measurements of this standard using faraday cups of 0.1739347 ± 20 (2SD). Furthermore, our result is consistent with that reported by Luguet et al. (2008) of 0.173926 ± 20 (2SD). Rhenium, Ir, Ru, Pt and Pd isotopic compositions for isotope dilution concentration determinations were measured using the Thermo Scientific iCAP Q ICP-MS. Total procedural blanks at EPL were less than 2 pg for Re, Os, Ir and Ru, 20 pg for Pd, and 30 pg for Pt.

4. Results

4.1. Petrography

The 16 xenoliths from Los Gemelos are fresh peridotites ~4–12 cm in size. Based on modal analysis, they are anhydrous clinopyroxene-poor lherzolites (LG-01 and LG-10), hydrous- (phlogopite-bearing LG-08 and LG-12) and anhydrous harzburgites (other samples) (Streckeisen, 1976) (Fig. S1 and Table S8). Olivine (59–84 vol%) and orthopyroxene (10–36 vol%) are the dominant phases in all samples, whereas clinopyroxene (2–9 vol%), spinel (1–5 vol%), and phlogopite (<1 vol%) occur in lower modal proportions (Table S8).

Peridotites from Los Gemelos are texturally equilibrated as indicated by triple point junctions (120°) and curvilinear grain boundaries (Fig. 2a). They display few deformation features with textures varying from medium to coarse protogranular, which is associated with the harzburgitic paragenesis mainly as a product of partial melting (Mercier and Nicolas, 1975) (Fig. 2a). Crystal sizes are 0.3 to 7.2 mm. Contacts between the xenoliths and the host alkaline-basalt are always straight with no evidence of basalt-peridotite interactions.

Olivine is generally subhedral and displays variable sizes (up to 5.7 mm). Large olivine crystals often exhibit fractures and kink-bands (Fig. 2b) and, occasionally, contain inclusions of spinel. *Orthopyroxene* is subhedral to anhedral and is larger with respect to other phases (3.3–7.2 mm) (Fig. 2a). In some samples, clinopyroxene exsolution lamellae occur along crystallographic controlled directions. *Clinopyroxene* is smaller than olivine and orthopyroxene (up to 2.3 mm), commonly occurring as anhedral crystals characterized by intense green color in textural equilibrium with the other minerals (Fig. 2a). Clinopyroxene crystals occur either as discrete grains or in clusters. *Spinels* vary in color from brown to reddish-brown. They are usually interstitial, ranging from amoeboid to vermicular shapes with sizes up to 1.7 mm (Fig. 2a, c). *Phlogopite* has sizes in the range of 0.4 and 1.3 mm and occurs as tabular isolated crystals or associated with spinel (in contact), sometimes as inclusions (Figs. 2c-f and 3a-d). The isolated phlogopite is larger, euhedral, and texturally equilibrated with peridotite assemblages (Figs. 2d-f and 3c-d). Conversely, phlogopite around and as inclusions in spinel crystals are smaller and subhedral (Figs. 2c, e and 3a-b). *Metasomatic glass veins* with hydraulic fracturing were found in samples LG-02, LG-06, LG-08, LG-12, LG-14, and LG-15 (Figs. 2b and 3e-f). These veins do not occur surrounding the mineral boundaries, that is, they are not an intergranular material.

4.2. Mineral chemistry

Individual measurements and the representative (average) compositions of olivine, orthopyroxene, clinopyroxene, spinel, phlogopite, and alkaline glass veins are given in Table S2. Negligible core-rim variation (<0.5 %) between the main oxides of mineral phases and alkaline veins was observed, so the average compositions were employed in the major element diagrams (Figs. 4 and S3-S4). Trace and REE concentrations were determined only for clinopyroxene and phlogopite (Table S3).

Olivine ($Fo_{0.90–0.91}$) is characterized by high Mg# (0.90–0.92; Mg# = Mg/(Fe + Mg) molar) and NiO content (0.37–0.43 wt%), coupled with CaO content below detection limit.

Chromium spinel has high Cr# (0.20–0.42; Cr# = Cr/(Cr + Al) molar) and Mg# between 0.67 and 0.80, defining a negative correlation between these parameters (Fig S2). This pattern indiates partial melting (Arai, 1987; Dick and Fisher, 1984). The only sample showing variation in spinel composition is LG-02, which is expressed by two different Al_2O_3 (43.45 and 37.87 wt%) and Cr_2O_3 (25.44 and 31.35 wt%) contents, resulting in variable Cr# (0.28 and 0.36) (Fig. S2).

Orthopyroxene is enstatite ($En_{0.90–0.91}$ $Fs_{0.08–0.09}$ $Wo_{0.07–0.10}$) with low Al_2O_3 (1.83–2.97 wt%), TiO_2 (below detection limit), and CaO (0.34–0.53 wt%) contents at a high Mg# (0.91–0.92) (Fig. S3).

Clinopyroxene is a high-Mg# (0.92–0.95) Cr-diopside (Cr_2O_3 = 0.72–1.71 wt%; $En_{0.47–0.50}$ $Fs_{0.03–0.04}$ $Wo_{0.47–0.49}$) with intermediate to high Ca/Al (molar) ratios (4.83–8.94) (Fig. 4 and Table S2). CaO contents and Ca/Al ratios show positive correlations with Mg# (Fig. 4). A negative correlation is observed in CaO vs. Al_2O_3 contents (Fig. 4). Increasing Mg# is accompanied by depletion in Al_2O_3 content in both pyroxenes (Figs. 4 and S3). Based on the primitive mantle-normalized trace and REE diagrams (Fig. 5), as well as on the presence or absence of phlogopite and glass veins, clinopyroxenes from Los Gemelos peridotites can be classified into three groups. Group 1 (G1) comprises xenoliths containing phlogopite (LG-08 and LG-12), and show fractionated LREE over HREE patterns (i.e., Ce/Yb_N = 8.79–10.11) (Fig. 5a). In contrast, Group 2 (G2: LG-02, LG-06, LG-14, LG-15) and especially

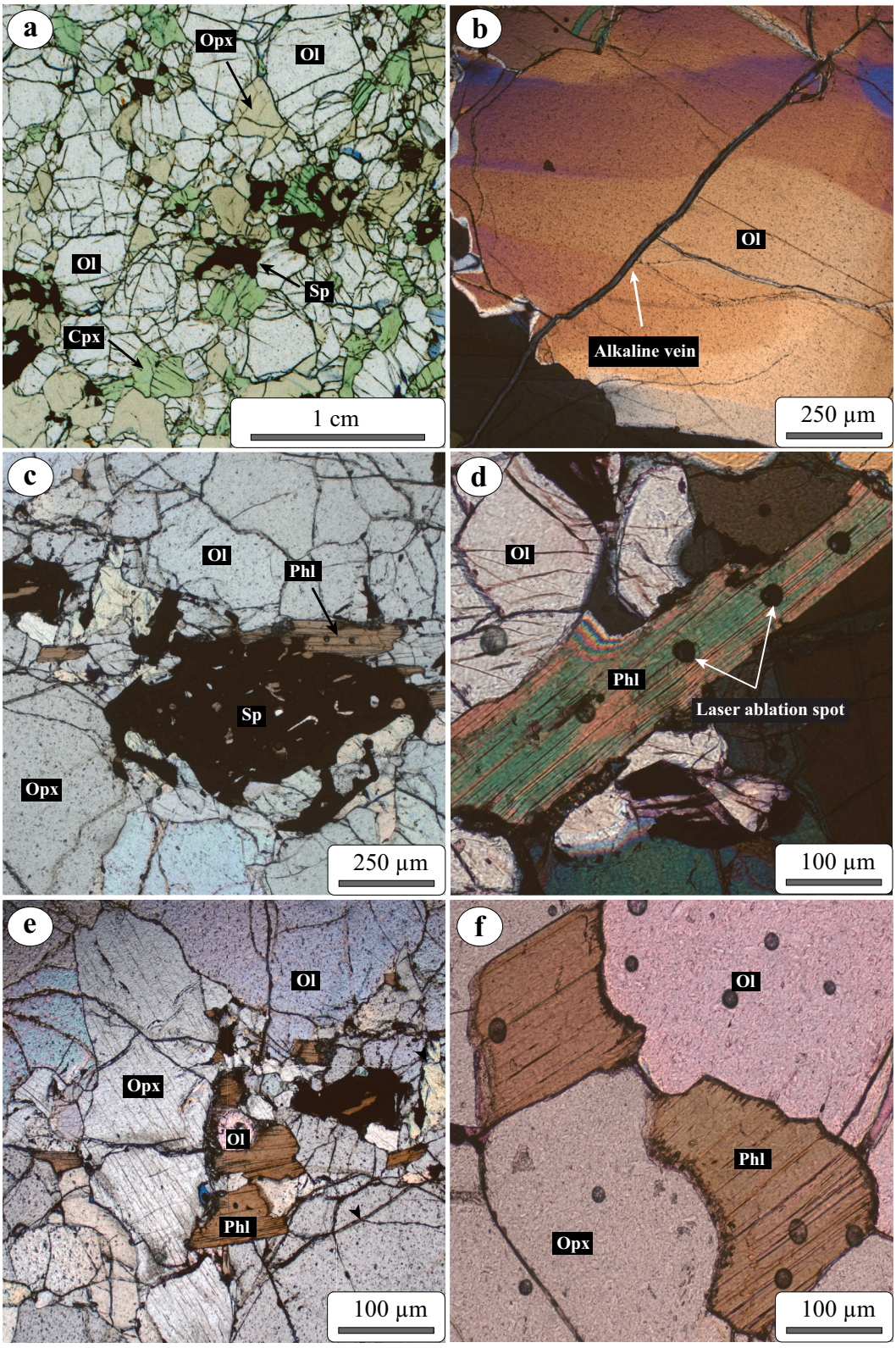

Fig. 2. Images showing the main mineralogical and textural features in mantle xenoliths from Los Gemelos. **(a)** Detail of a scanned image from a thin section showing the representative mineral assemblage of olivine (Ol), orthopyroxene (Opx), clinopyroxene (Cpx), and spinel (Sp) (sample LG-10). **(b)** Photomicrograph (crossed polars) of a well-developed vein of adakite composition crosscutting an olivine crystal (sample LG-06). **(c)** Photomicrograph highlighting phlogopite crystals as inclusions and around spinel grains (sample LG-12). **(d)** Photomicrograph (crossed polars) of a euhedral phlogopite crystal in which the hole trail represents the laser ablation in the ICP-MS (sample LG-08). **(e-f)** Photomicrographs showing the localized occurrence of phlogopite as euhedral crystals and as inclusion in spinel (samples LG-12 and LG-08, respectively).

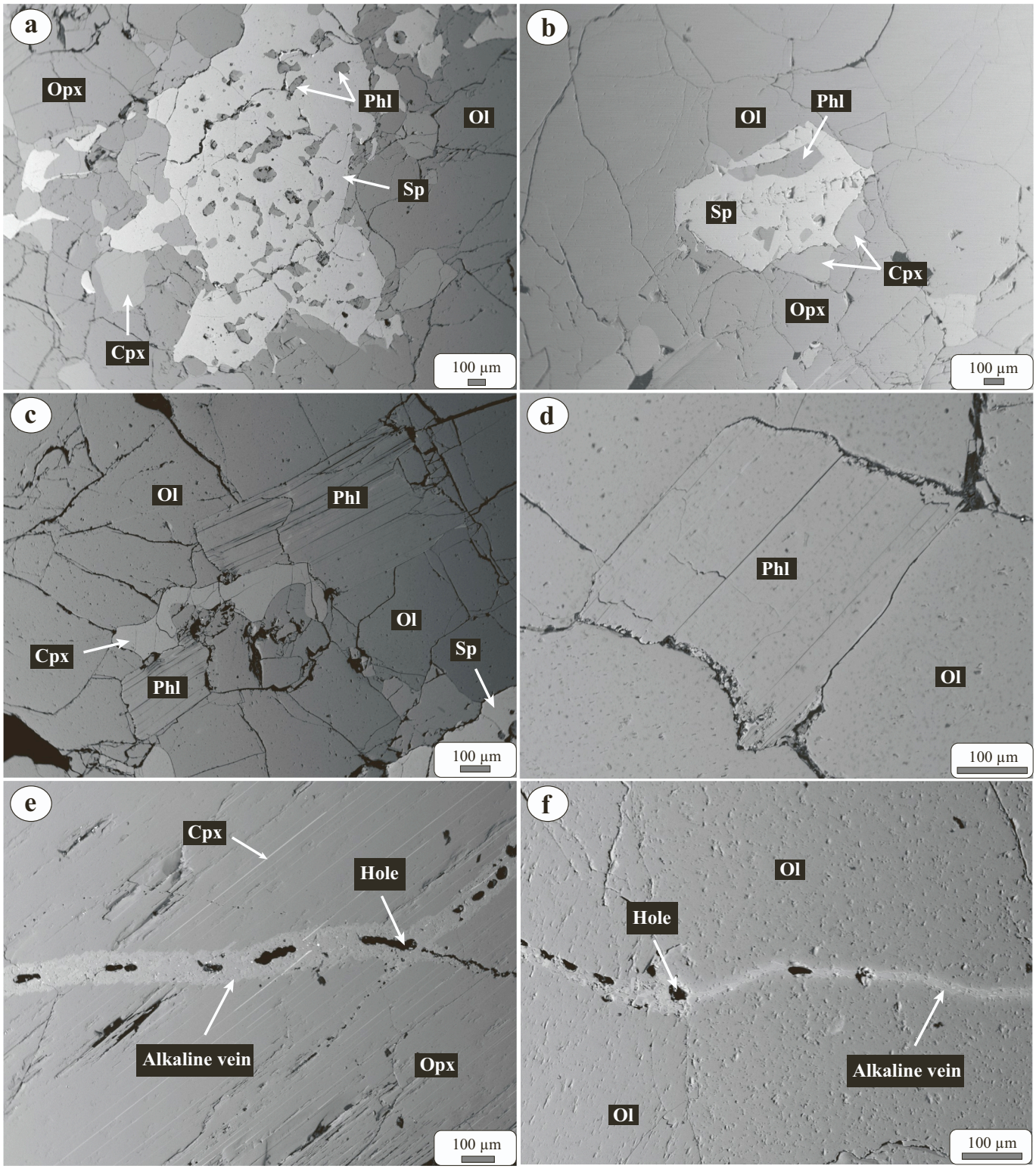

Fig. 3. Backscattered electron images (BSE) of glass veins with adakite composition and phlogopites (Phl), which define modal metasomatism. **(a-b)** Spinel (Sp) crystals containing abundant silicate inclusions, as phlogopite (sample LG-08). **(c-d)** Euhedral phlogopite crystals (sample LG-08). **(e-f)** Adakite glass veins with variable thicknesses crosscutting, respectively, orthopyroxene (Opx) (sample LG-02) and olivine (Ol) (sample LG-06). Orthopyroxene has clinopyroxene exsolution lamellae. The black areas within adakite veins are holes produced by polishing of the thin section.

Group 3 (G3: LG-03, LG-09, LG-11, LG-16) have spoon-like REE patterns defined by depletion from HREE to Pr (i.e., Pr/Yb_N = 0.01–0.25) with selective enrichment from Pr to LREE (i.e., La/Pr_N = 1.50–6.89) (Fig. 5a). These two groups show Ce/Yb_N ratios lower than 0.32. Glass veins were only observed in xenoliths from G1 and G2. In the PM-normalized trace element diagram, clinopyroxenes have positive anomalies of W, U, La, Pb, Mo (except for G1 xenoliths), and Eu, with negative anomalies of Rb, Ba, Th, K, Zr, Hf, and Ti (Fig. 5b). Niobium and Ta negative anomalies are identified in samples from G1 and G2 (especially in the former), but G3 do not show clear depletion in these

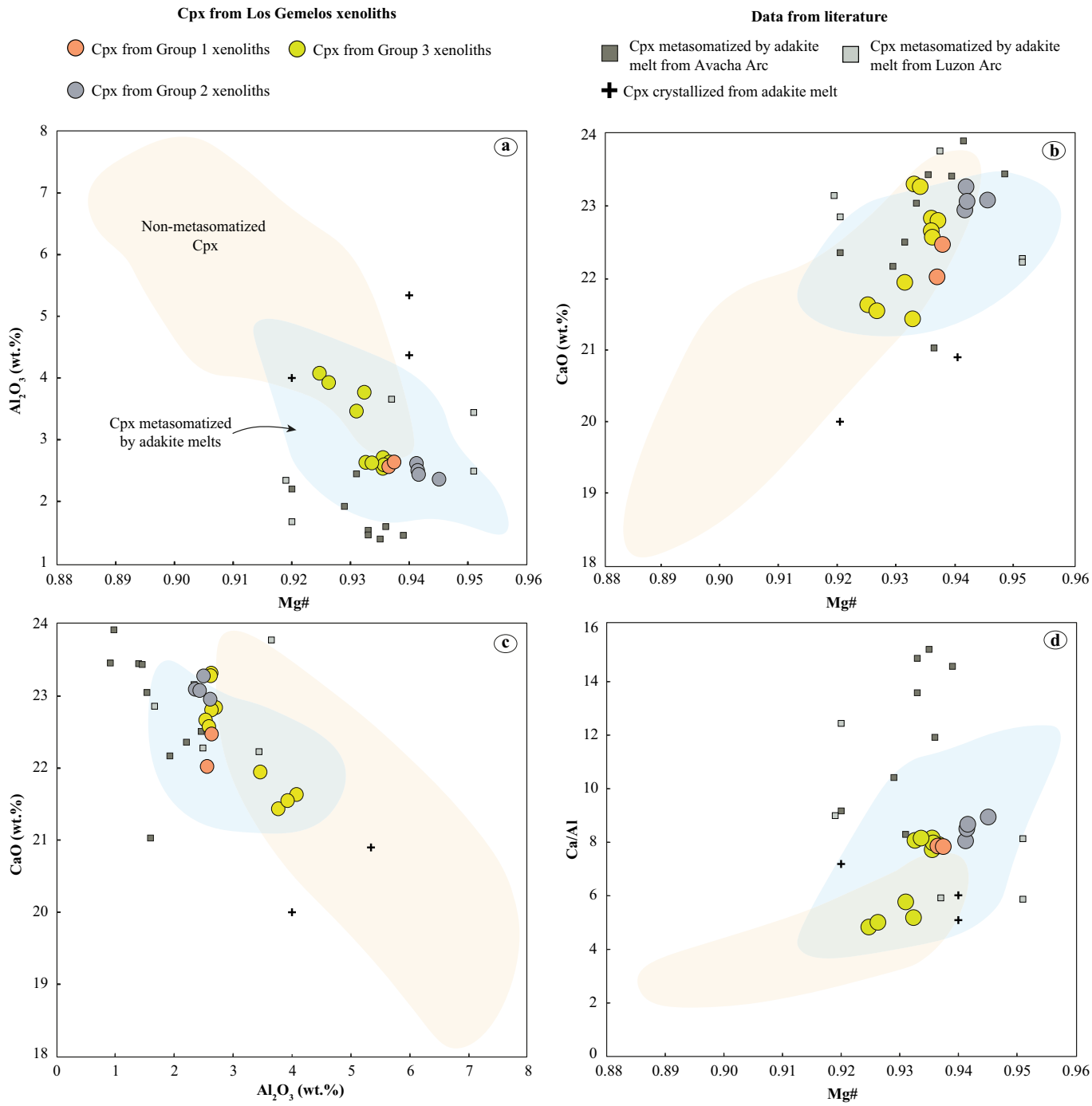

Fig. 4. Selected major elements (Al_2O_3, TiO_2, CaO, and Ca/Al) vs. Mg# (a-d) and Al_2O_3 vs. CaO (e) of clinopyroxenes (Cpx) from Los Gemelos. Our samples show compositional affinity with clinopyroxenes metasomatized by adakite melts (light blue field) of mantle xenoliths from Cerro de los Fraile and Paso de Indios region (Faccini et al., 2013; Bertotto et al., 2021). The field defined for non-metasomatized clinopyroxenes from Patagonia (light yellow) includes mantle xenoliths from Agua Poca, Huanul, and Tres Lagos (Ntaflos et al., 2007; Bertotto et al., 2013, 2022). For comparison, were plotted clinopyroxenes metasomatized by adakite melts from Avacha and Luzon arcs (Arai et al., 2003, 2004; Ishimaru et al., 2007), and experimentally crystallized by adakite melts (Corgne et al., 2018). (For interpretation of the references to color in this figure legend, the reader is referred to the web version of this article.)

elements (Fig. 5b). Although there are no clinopyroxene REE data for some xenoliths (LG-01, LG-04, LG-05, LG-07, LG-10, LG-13), they were included in G3 according to their clinopyroxene major element distribution (Fig. 4), and lack of glass veins and phlogopite.

Phlogopite is restricted to xenoliths LG-08 and LG-12, showing homogeneous composition in all petrographic types (Table S2). Fig. 6 shows strong enrichment of LREE over HREE (Ce/Yb_N = 15.32–22.08) with enrichment in incompatible elements (i.e., Cs, Rb, Ba, K, Pb, Mo, Sr, and Li), and in high field strength elements (HFSE, Nb-Ta-Ti) compared to REEs and Th.

Glass veins (Figs. 2b and 3e-f) are widespread in spinel peridotites from G1 and G2. They have bimodal composition marked by high- and low-SiO_2 contents (Fig. S4). High-SiO_2 glass veins have a compositional affinity with typical adakites as demonstrated by their high SiO_2 (60.38–61.29, adakite >56 wt%), Al_2O_3 (15.78–16.52 wt%, adakite >15 wt%), and Na_2O (4.40–4.54 wt%, adakite >3 wt%), coupled with low MgO (2.26–2.37 wt%, adakite <3 wt%) (Defant and Drummond, 1990; Martin et al., 2005; Castillo, 2012 and references therein)

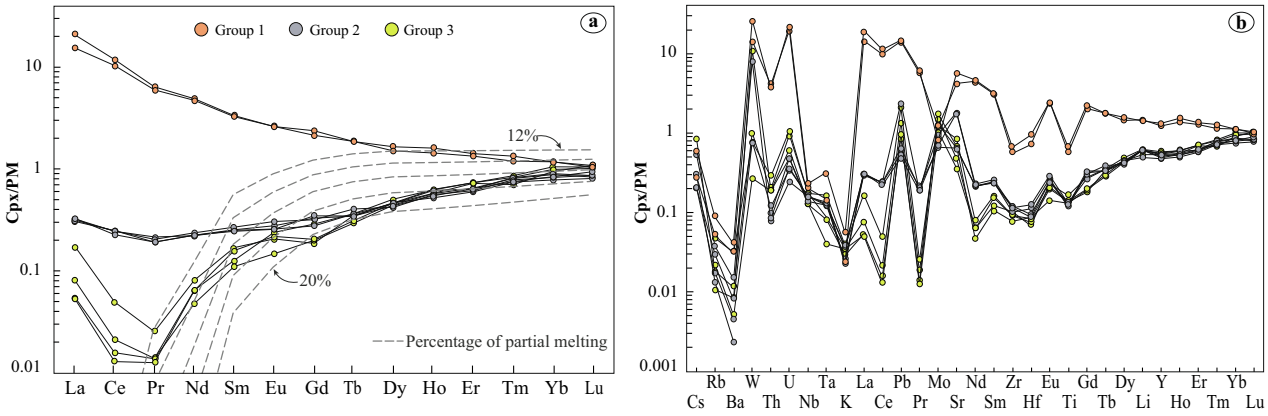

Fig. 5. Rare earth element (a) and multielement (b) diagrams of clinopyroxenes (Cpx) from Los Gemelos. Concentrations are normalized to the primitive mantle (PM, Sun and McDonough, 1989). Partial melting estimates from 12 to 20 % are indicated by dashed lines with the increment of 2 % in (a). Details about the calculations are in the main text.

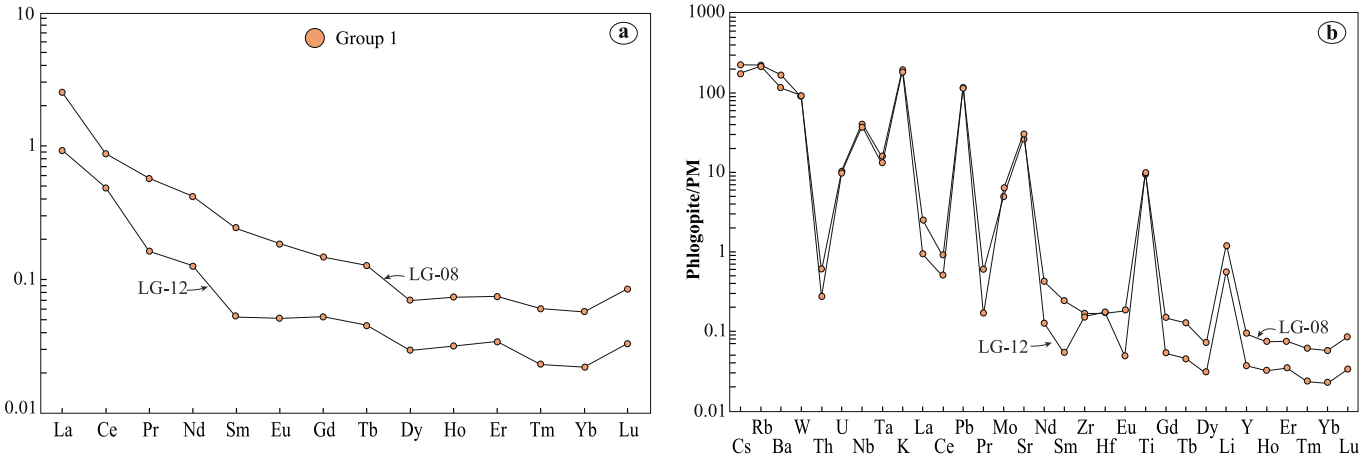

Fig. 6. Rare earth element (a) and multielement (b) diagrams of phlogopites from Los Gemelos. Concentrations are normalized to the primitive mantle (PM, Sun and McDonough, 1989).

(Fig. S4a-c and Table S2). In contrast, low-SiO_2 glass veins (48.75–50.93 wt%) are coupled with high Al_2O_3 (16.56–17.62 wt%), Na_2O (4.14–5.32 wt%) and MgO (4.43–4.85 wt%) contents (Fig. S4a-c and Table S2). Both types of glass have high K_2O (2.84–4.37 wt%, Fig. S4d), and high alkali contents ($K_2O + Na_2O$ = 7.37–9.59 wt%) compared to adakite lavas from Patagonia (K_2O < 2.7 wt% and alkalis <7.0 wt%; Mahlburg Kay et al., 1993; Stern and Kilian, 1996; Ramos et al., 2004) (Fig. S4 and Table S2). The high K_2O content of these veins results in high K_2O/Na_2O ratios (0.63–0.84, adakite <0.5). Another element with anomalous high content compared with typical adakites is TiO_2 (2.20–2.91 wt%) (Fig. S4e). In general, CaO and FeO are higher in low-SiO_2 glass (CaO = 5.82–12.14 wt%, FeO = 5.11–7.18 wt%) compared to those of high-SiO_2 (CaO = 4.75–5.73 wt%, FeO = 2.68–3.46 wt%) (Fig. S4f-g). Samples LG-14 and LG-15 are characterized by the occurrence of both types of glass (high- and low-SiO_2), suggesting the infiltration of a heterogeneous metasomatic agent.

4.3. Temperature estimates

Temperature estimates were obtained using several geothermometers from the PTEXL Excel spreadsheet (Stachel, 2022, "PTEXL - Geothermobarometry of Mantle Rocks", https://doi.org/10.5683/SP3/IMYNCL, Borealis, V2) (Table S8) assuming 1.5 GPa (spinel-facies).

Here we employed accurate and robust geothermometers based on two-pyroxenes (Brey and Köhler, 1990; Taylor, 1998) and Ca in orthopyroxene (Brey and Köhler, 1990; Nimis and Grütter, 2010). The temperature average of each sample will be considered below (739–953 °C) (Table S8).

4.4. Whole-rock geochemistry

Whole-rock major and trace element contents were determined for the largest samples (n = 9, Table S4). These results do not show the same compositional distinctions according to which groups were defined based on clinopyroxene mineral chemistry. In terms of major elements, Los Gemelos peridotites have high-Mg# (0.91–0.92), as well as variable and low CaO (0.74–2.07 wt%) and Al_2O_3 (0.83–1.80 wt%) contents (Table S4). Negative correlations observed between MgO vs. CaO, Al_2O_3, Na_2O, and TiO_2 are typical of melt extraction processes (Fig. S5).

In general, all analyzed samples display selective LREE enrichment (e.g., La/Sm_N = 1.34–6.31), and U-shaped REE pattern with variable depletion of MREE relative to LREE and HREE ($La/Sm_N > 1$ and $Gd/Yb_N < 1$; Fig. 7a, Table S4). Sample LG-07 has the highest HREE content (Lu_N = 0.41) and shows a continuous decrease from Lu to Nd (Nd/Lu_N = 0.13) and an increase from Pr to La (La/Pr_N = 1.89). Sample LG-01 also has a U-shaped REE pattern with one of the lowest HREE and the highest LREE contents, with a progressive enrichment from Dy to La (La/Dy_N = 18.17).

Regarding the PM-normalized trace element diagram (Fig. 7b), most samples have positive Pb anomalies and smaller ones in Cs, Ba, La, and

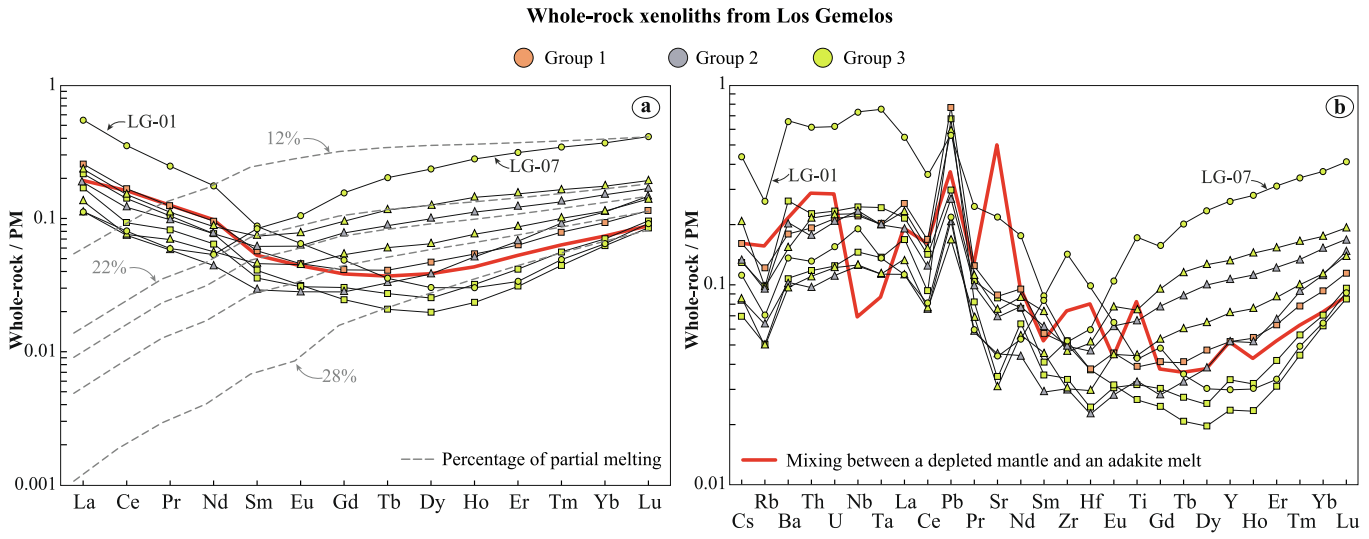

Fig. 7. Rare earth element (a) and multielement (b) diagrams of whole-rock samples from Los Gemelos. Concentrations are normalized to the primitive mantle (PM, Sun and McDonough, 1989). Partial melting estimates (dashed lines) are indicated in 12 %, as well as from 22 to 28 % with the increment of 2 % in (a). Details about the calculations are in the main text. Samples LG01 and LG-07 are highlighted due to their distinct compositional patterns. For comparison, the trace and rare earth elements patterns of a mixing model between a depleted mantle (99.5 %) and an adakite melt (0.5 %; Corgne et al., 2018) were used to reproduce the compositional patterns of Los Gemelos peridotites (see section 5.1 for details).

Eu. On the other hand, negative anomalies are observed in Rb, Sr, and Hf (Fig. 7b). Sample LG-07 has positive anomalies of Cs, Ba, Nb, Pb, and Ti coupled with negative anomalies of Rb, Sr, Zr, and Hf. Finally, sample LG-01 shows positive anomalies of Cs, Ba, Nb, Ta, Pb, Zr and Hf, coupled with a negative anomaly of Rb (Fig. 7b).

4.5. Re—Os isotope compositions and highly siderophile elements

Six whole-rock peridotites were analyzed for Re—Os isotopes and HSE contents (Table S5). Initial $^{187}Os/^{188}Os$ ratios were calculated considering the eruption age of the host basalt (0.45 ± 0.03 Ma; Table S1). The γOs values (−3.5 to −6.4, where γOs =

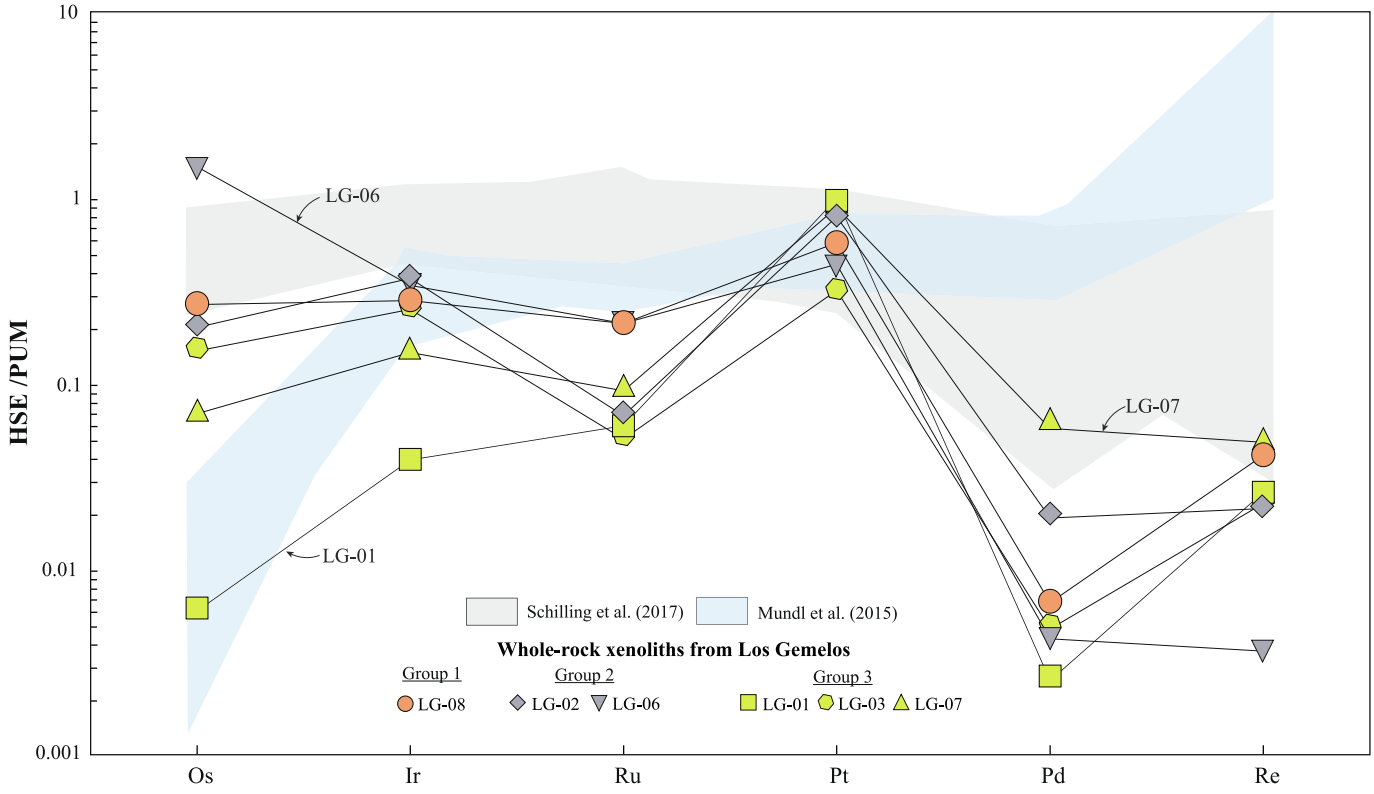

Fig. 8. Primitive Upper Mantle (PUM, Becker et al., 2006) normalized highly siderophile element (HSE) patterns of the Los Gemelos peridotites. Samples LG-01, LG06, and LG-07 are highlighted due to their distinct patterns. In general, the xenoliths present typical partial melting pattern characterized by depletion of Pd and Re coupled with relative enrichment of Os Ir, and Ru. Platinum is enriched in all samples. Compared with the SCLM beneath the Deseado Massif (Mundl et al., 2015; Schilling et al., 2017), Los Gemelos shows depletion in Ru, Pd and Re, indicating a highly-depleted mantle.

$((^{187}Os/^{188}Os)_{sample}/(^{187}Os/^{188}Os)_{PUM}-1) \times 100$, where PUM = primitive upper mantle; Walker et al., 1989; Meisel et al., 2001), calculated based on the initial Os ratios, are compatible with Re-depleted residues. The Re-depletion model ages (T_{RD}) of five samples range from 1.1 to 0.9 Ga (Grenville-age) while sample LG-07 yields a younger age of 0.6 Ga. Also, most samples have mantle model ages (T_{MA}) only slightly older (1.3–1.1 Ga) than their T_{RD} model ages, reflecting their low Re/Os ratios. In contrast, samples LG-01 and LG-07 have T_{MA} significantly different than their T_{RD}, suggesting recent addition of Re.

Overall, well-defined positive correlations between $^{187}Os/^{188}Os$ vs. whole-rock Al_2O_3 (wt%) and Yb_N are observed (Fig. S6). The $^{187}Os/^{188}Os$ vs. Al_2O_3 correlation extrapolates to 0.11819 at $Al_2O_3 = 0$, providing a T_{RD} model age of 1.55 Ga, slightly older than the T_{RD} of the individual samples. In contrast, $^{187}Os/^{188}Os$ vs. Os (ppb), Ol Mg#, and Sp Cr# define negative correlations (Fig. S6). The HSE (PGEs + Re) concentrations (in ppb) of Los Gemelos mantle xenoliths vary widely (Os = 0.024–5.854, Ir = 0.139–1.319, Ru = 0.360–1.510, Pt = 2.468–7.707, Pd = 0.018–0.416, and Re = 0.001–0.017) (Fig. 8 and Table S5). Except for the Os_N (1.50) and Pt_N (1.01) contents of LG-06 and LG-01, respectively, all samples are depleted compared to the PUM-normalized HSE values (Becker et al., 2006) (Fig. 8). In addition, most samples have similar HSE patterns, with variable depletion of Pd compared to Os, Ir and Ru, reflecting different degrees of partial melting, and positive anomalies of Pt (Fig. 8 and Table S5). Sample LG-01 shows anomalously low Os and Ir, but Re concentrations similar to the other xenoliths leading to its anomalously high Re/Os ratio. Sample LG-06 shows enrichment of Os ($Os_N/Ir_N = 4.35$) (Fig. 8 and Table S5). Samples LG-01, LG-03 and LG-08 have relatively high Re_N/Pd_N ratios (4.7–10.3).

5. Discussion

5.1. Partial melting of Los Gemelos mantle xenoliths

Clinopyroxene-poor spinel peridotites from Los Gemelos show petrographic (e.g., presence of phlogopite and alkaline glass veins) and chemical evidence of a complex mantle evolution involving melt extraction (depletion) followed by enrichment (metasomatism). After partial melting, residual peridotites are expected to range from fertile lherzolites to highly refractory clinopyroxene-poor peridotites characterized by low whole-rock Al_2O_3 and CaO contents, high forsterite content in olivine, and Cr-rich spinel. Typical negative correlations between MgO vs. basaltic elements (e.g., CaO, Al_2O_3, Na_2O, and TiO_2), which are expected in the solid residue after partial melting, are observed in whole-rock geochemistry (Fig. S5). Most samples also show relative depletion of the more incompatible Re and Pd compared to the compatible Ir and Os, consistent with them being residues of melt extraction. Comparing with previous results reported for the SCLM beneath the Deseado Massif (Mundl et al., 2015; Schilling et al., 2017), our samples record depletion in Ru, Pd, and Re (Fig. 8), suggesting a highly-depleted lithosphere beneath Los Gemelos. The positive $^{187}Os/^{188}Os$ vs. Al_2O_3 correlation indicates that this melt extraction occurred well before the event that brought the xenoliths to the surface with T_{RD} ages in the range of a billion years. Whole-rock MREE/HREE ratios support partial melting (i.e., $Sm/Yb_N = 0.23–0.65$; except for LG-01 = 1.35) (Table S4). Some aspects of mineral chemistry provide further evidence of depletion, such as the high Cr# of spinels (0.20–0.42) and Mg# of the silicate phases (0.90–0.95) (Table S2). Well-defined negative correlations between Mg# vs. Al_2O_3 and TiO_2 (for both pyroxenes), and CaO vs. Al_2O_3 (for clinopyroxene), besides the positive correlations observed of Mg# vs. CaO and Ca/Al (molar) for clinopyroxene (Figs. 4 and S3) attest to extraction of partial melts.

Partial melting degrees were estimated based on whole-rock and clinopyroxene HREE compositions (i.e., Yb and Lu). For whole-rock, this modelling yielded between 22 and 28 % of partial melting (Fig. 7a). Xenolith LG-07 shows 12 % of partial melting, likely an underestimation compared to the other samples. More likely, this result reflects the influence of later metasomatism. In comparison, the melting model using clinopyroxene requires between 16 and 17 % of partial melting (Fig. 5a), which is lower than whole-rock estimates.

5.2. Timing of partial melting and metasomatism (Re addition)

According with modal, mineral and whole-rock compositions, Los Gemelos peridotites are depleted residues after high degrees of melt extraction (16–28 %) in the spinel-stability field. In this context, HSE and Re are preferentially retained by sulfides. However, at high degrees of partial melting (>20 %) these minerals are completely consumed in the melt (e.g., Mundl et al., 2016 and references therein). Consequently, the solid residue will be selectively depleted in Re, Pd, and Pt (the latter to a lesser extent), whereas Os, Ir, and Ru will be preferentially retained in alloys in the residual peridotite (Pearson et al., 2004). Kepezhinskas and Defant (2001) associated the selective mantle enrichment of Pt relative to their adjacent elements (Ru and Pd) to melt extraction in the back-arc of Kamchatka. In this scenario, refractory Pt—Fe alloys selectively concentrate Pt relative to Ru and Pd and, therefore, increase the Pt/Ru and Pt/Pd ratios in the mantle wedge. Thus, the high PUM-normalized ratios between Os, Ir, and Ru over Re and Pd (values >1) observed in Los Gemelos xenoliths, as well as the enrichment of Pt compared to Ru and Pd, probably reflect the preferential retention of Pt—Fe alloys after high degrees of partial melting (Fig. 8). However, there are two exceptions to this tendency, where sample LG-01 is enriched in Re relative to Os ($Re_N/Os_N = 4.35$) and sample LG-06 that is enriched in Os with respect to Pt ($Os_N/Pt_N = 3.35$) (Fig. 8).

The Re/Os ratio of LG-01 is higher than PM. This is a typical signature of metasomatism by a *Re*-rich, Os-poor melt whereas the high Os/Pt of LG-06 is the more common signature of melt depletion, as Pt is generally more incompatible than Os during mantle melting (e.g., Pearson et al., 2004). The much lower Re/Os ratios than PM of all samples, except LG-01 and LG-07, are a typical signature of melt-depleted peridotites (e.g., Walker et al., 1989). The sub-PM $^{187}Os/^{188}Os$ isotopic compositions of all samples indicate that this depletion occurred well before the volcanic event that brought these samples to the surface, with T_{RD} model ages averaging 0.97 ± 0.39 Ga (2SD) for all Los Gemelos samples. Leaving out the data for the two samples with higher Re/Os, the average T_{RD} of the remaining samples is 1.09 ± 0.04 Ga and the average T_{MA} of these four samples is 1.22 ± 0.10 Ga, suggesting that the initial melt depletion occurred about 1.2–1.1 Ga and that metasomatic addition of Re was insufficient to greatly disturb their Re—Os systematics. Additionally, the positive correlations between $^{187}Os/^{188}Os$ vs. whole-rock Al_2O_3 (wt%) that extrapolates to 0.11819 at $Al_2O_3 = 0$, suggest that the partial melting event occurred at the beginning of the Mesoproterozoic (1.55 Ga).

Sample LG-07 has a Re/Os ratio (0.06) only slightly lower than the PM value (0.09), which might indicate that it was less depleted by melt extraction, though this is not supported by its major and trace element characteristics. The Re/Os ratio of sample LG-01 is much higher than PM, which is inconsistent with its sub-PM $^{187}Os/^{188}Os$, and most likely reflects addition of Re by recent metasomatism. Rough bounds can be placed on when this metasomatism might have occurred by noting that, given its Re/Os ratio, the Os isotopic composition would increase from the lowest measured for any sample from Los Gemelos ($^{187}Os/^{188}Os = 0.12134$) to the measured isotopic composition of LG-01 in 60 Ma, which likely provides an upper limit to the time of metasomatism.

5.3. Characteristics and origin of metasomatism

In this section we will address the metasomatic vestiges recorded by Los Gemelos mantle xenoliths.

5.3.1. Phlogopite as an expression of modal metasomatism

In Patagonia, phlogopite is found in mantle xenoliths from the

Gobernador Gregores (Gorring and Kay, 2000; Laurora et al., 2001; Rivalenti et al., 2004; Bjerg et al., 2005) and Pali-Aike Volcanic Field (PAVF, Stern et al., 1999; Jalowitzki et al., 2016). In PAVF, the Rb—Sr isochron age of 13.6 ± 0.8 Ma revealed that phlogopite crystallization occurred simultaneously with the subduction of the Chile Ridge (Jalowitzki et al., 2016). Thus, the existence of phlogopite attests to the transfer of volatiles possibly released from the subducted oceanic crust to the overlying mantle wedge.

5.3.2. *Cryptic enrichment traced with hypothetical melts in equilibrium with clinopyroxene*

Compared to the other peridotites from Los Gemelos, harzburgites containing phlogopite (G1: LG-08 and LG-12) show distinctive clinopyroxene REE patterns (LREE>HREE) and strong depletions of Nb—Ta, Zr—Hf and Ti, coupled with pronounced enrichment of W, U, Pb, Sr, and Eu (Fig. 5).

To estimate the possible composition of the melt (metasomatic agent) in equilibrium with these clinopyroxenes, we applied the model proposed by Ionov et al. (2002), as well as their clinopyroxene/melt partition coefficients. Based on the trace element patterns, interaction between these clinopyroxenes and the host basalt is rejected (Fig. S7a-b). Nevertheless, the calculated metasomatic melts share some compositional affinity with natural glass-filled veins and calculated primary melt from Cerro del Fraile (Kilian and Stern, 2002). They also display strong similarity with the adakite lavas from Cerro Pampa (Corgne et al., 2018), Southern Chile Trench sediments (i.e., Kilian and Behrmann, 2003), and with calc-alkaline lavas from the Maca and Cay stratovolcanoes (D'Orazio et al., 2003). While Ti, Zr and Hf are possibly affected by subsolidus re-equilibration between the pyroxenes (Rampone et al., 1991), the negative anomalies of Nb—Ta in the hypothetical melt in equilibrium with Los Gemelos clinopyroxenes would be entirely consistent with an adakitic metasomatic melt (Fig. S7b), possibly hybridized with depleted peridotite and Chile Trench sediments.

We note that the spoon-shaped REE patterns of G2 and G3 samples point to chromatographic enrichment (Bodinier et al., 2004), precluding meaningful interpretation of calculated hypothetical melts, whereby G2 samples have reached a greater degree of equilibrium with the metasomatic melt than G3 samples (Fig. S7c-d). We attribute the crystallization of phlogopite, as well as the distinctive clinopyroxene trace element pattern in hydrated harzburgites, to their deeper origin compared to the other xenoliths. In this way, the intensity of metasomatism decreases toward the shallower SCLM, defining chromatographic fractionation and reaction process at decreasing melt mass.

5.3.3. *Mineral compositional constraints on the nature of metasomatism*

To constrain the imprint of the metasomatic agents described above on the chemical composition of the Los Gemelos xenoliths, the mineral chemistry results of ortho- (Fig. S3) and clinopyroxenes (Fig. 4) were compared with typical non-metasomatized (depleted) (Ntaflos et al., 2007; Bertotto et al., 2013, 2022) and adakite-metasomatized (Faccini et al., 2013; Bertotto et al., 2021) pyroxenes from other xenolith localities in Patagonia. Depleted samples are from Agua Poca, Huanul and Tres Lagos, while the metasomatized xenoliths are from the Cerro del Fraile and Paso de Indios region. We also used for the major and trace elements plots (when these studies contain the selected elements), the pyroxenes metasomatized by adakite melts from an experimental study (Corgne et al., 2018), and natural pyroxenes from the Avacha arc (Arai et al., 2003; Ishimaru et al., 2007) and Luzon arc (Arai et al., 2004).

Depleted pyroxenes should be characterized by high Mg# (usually >90) coupled with low concentrations of basaltic elements. However, the metasomatism caused by the percolation of adakite melts produces a similar effect (Figs. 4 and S3). For this reason, although pyroxenes from G2 and G3 plot within the fields of samples affected by adakite metasomatism (Figs. 4 and S3), we prefer to be careful with the interpretation of these results. This assumption is justified by the absence of phlogopite in these samples (G2 and G3), as well as by the significant difference of their clinopyroxene REE and extended trace element patterns compared to those from G1 (Fig. 5). Phlogopite-bearing harzburgites (G1) show similar composition with xenoliths metasomatized by adakite melts from Patagonia, Avacha, and Luzon (Fig. 4 and S3). In general, these samples also plot within the experimental results of pyroxenes characterized by enrichment promoted by interaction with adakite melt, although these experiments have slightly higher Al_2O_3 and TiO_2 coupled with lower CaO contents. Thus, interaction with a small volume of slab-derived melt from a hydrous eclogitic protolith (adakite) was insufficient to significantly modify the highly-depleted character revealed by major elements (Fig. 4).

Regarding trace and rare earth element contents of clinopyroxenes, Fig. 9 correlates La/Yb_N vs. Sr/Y (a) and Ti/Eu (b), as well as Sr (ppm) vs. Ti/Eu (c). The selection of these elements is justified due to the preferential enrichment of La, Sr and Eu coupled with depletion of Yb, Y, and Ti during metasomatism caused by percolation of eclogite-derived adakite melt into the mantle wedge. In Fig. 9, the strong affinity of G1 clinopyroxenes from Los Gemelos with adakite melts is confirmed. They plot within the field of clinopyroxenes from Patagonia (Faccini et al., 2013; Bertotto et al., 2021) and the Avacha arc (Ishimaru et al., 2007), sometimes overlapping or toward the composition of glass veins from Cerro del Fraile (Kilian and Stern, 2002) (Fig. 9). Due to their less enriched character regarding incompatible trace elements, clinopyroxenes from G2 and G3 mainly resemble the field of depleted peridotites from Patagonia (Ntaflos et al., 2007; Bertotto et al., 2013, 2022) (Fig. 9). This observation suggests that these two compositional groups were less affected by calc-alkaline (adakite?) or alkaline metasomatism.

5.3.4. *Bulk compositional evidence for subduction-related metasomatism*

Regarding the whole-rock geochemistry, distinctive elemental characteristics are usually promoted by reactions between adakite melts and peridotites, such as enrichment of key elements (i.e., Pb, Sr, Zr, Hf, and LREE/HREE) and depletion of Nb—Ta (e.g., Defant and Drummond, 1990; Stern and Kilian, 1996; Kilian and Stern, 2002; Martin et al., 2005; Fallon et al., 2008; Corgne et al., 2018). In general, Los Gemelos peridotites with U-shaped REE patterns lack the typical positive anomalies of Sr, Zr, and Hf, as well as negative anomalies of Nb—Ta, characteristics of adakites (except for few samples with negative Ta and positive Zr anomalies) (Fig. 7b). The U-shaped REE pattern can be explained by addition of a low amount of a LREE-enriched melt (adakite or alkaline) to a strongly LREE-depleted lithosphere. This generates the selective enrichment of LREE abundances, whereas the MREE and HREE will maintain the signature of past melt depletion. To reproduce the U-shaped REE pattern of Los Gemelos peridotites, we modelled mixing between a depleted mantle after 28 % of partial melting from a PM composition (see section 5.1) and an adakite melt from Cerro Pampa (Corgne et al., 2018) (in the proportion of 99.5 and 0.5 %, respectively) (Fig. 7). The REE pattern of this mixture matches that observed in the whole-rock composition of the Los Gemelos peridotites (Fig. 7a). The modelled trace element pattern presents the typical compositional patterns of adakite metasomatism (Fig. 7b). Hence, the metasomatic overprint in the Los Gemelos peridotites was enough to significantly add LREE to a starting depleted peridotite to change the REE pattern, but not enough metasomatic agent was added to significantly influence the abundance of all these other elements. Therefore, the lack of positive anomalies of Sr, Zr, and Hf coupled with negative anomalies of Nb—Ta probably reflects an inherited characteristic that was not effectively modified by the metasomatism. Alternatively, these discrepancies observed in Nb patterns can be associated to analytical aspects in which Nb shows lower precision (44 %) compared to other trace elements (see Supplementary Information).

Still considering the whole-rock geochemistry, samples LG-01 and LG-07 clearly have distinct patterns (Fig. 7), probably implying a complex and different interaction between metasomatic agent and residual peridotite. Although these two samples do not exhibit modal metasomatism, their higher Re/Os suggests that they contain more of the

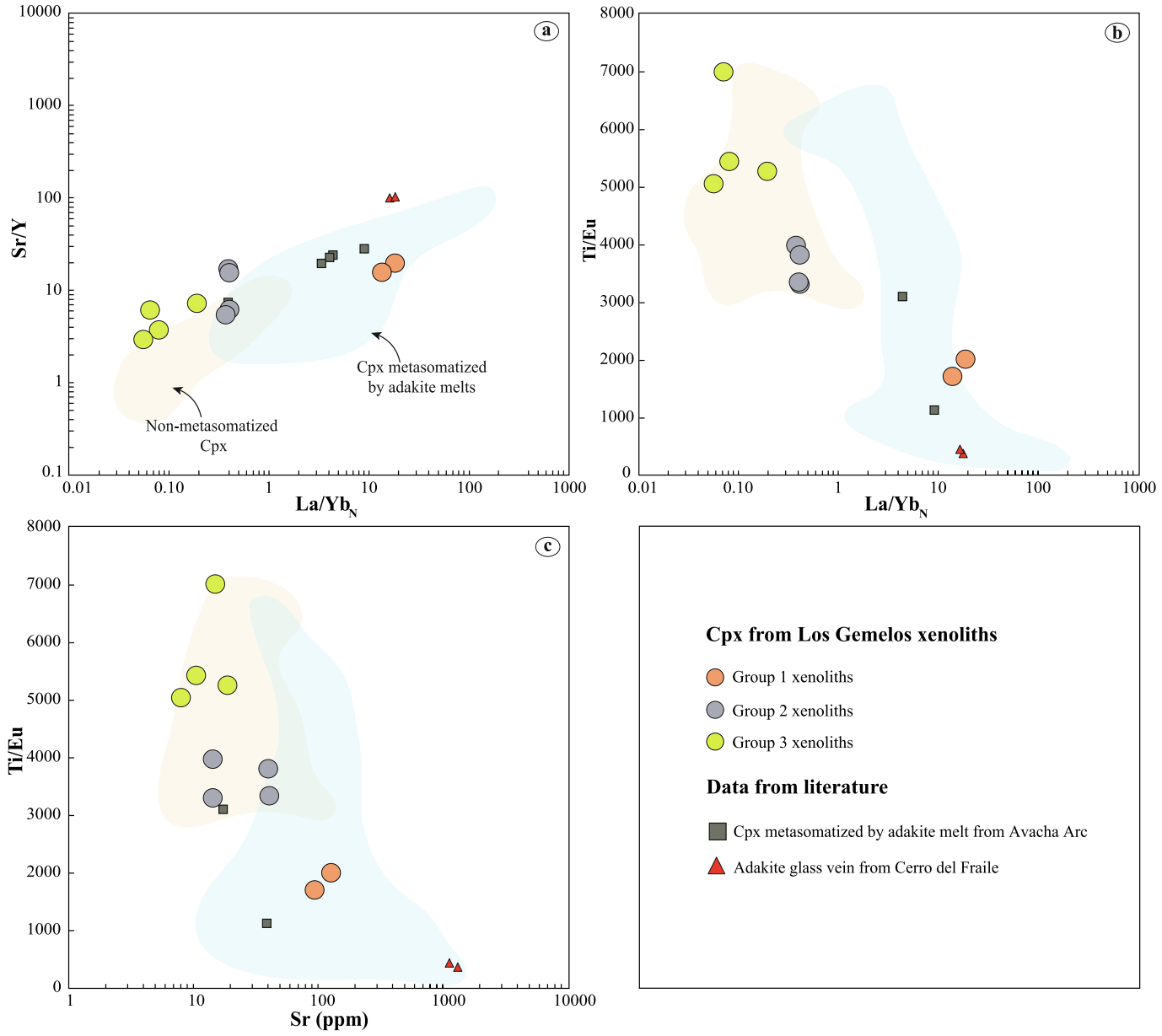

Fig. 9. La/Yb$_N$ vs. Sr/Y (a) and Ti/Eu (b), and Sr (ppm) vs. Ti/Eu (c) diagrams of clinopyroxenes (Cpx) from Los Gemelos peridotites. Only Group 1 samples (those containing phlogopite) record clear compositional affinity with clinopyroxenes metasomatized by adakite melt from Avacha (Ishimaru et al., 2007), as well as with glass veins with adakite composition from Cerro del Fraile (Kilian and Stern, 2002). Group 2 clinopyroxenes from Los Gemelos show less evident correlation, whereas those from Group 3 lack compositional affinity with metasomatic process. This observation indicates decoupling between major and trace elements (see Fig. 3 for comparison and the main text for discussion). Fields defined by non-metasomatized (light yellow) and metasomatized (light blue) peridotites from Patagonia are the same as in Fig. 4. The La/Yb ratio is normalized ($_N$) to the primitive mantle (Sun and McDonough, 1989). (For interpretation of the references to color in this figure legend, the reader is referred to the web version of this article.)

metasomatic component than do the other samples.

5.3.5. *Glass-filled veins*

Another expression of metasomatism recorded by mantle xenoliths from Los Gemelos is the occurrence of crosscutting networks of veins apparently filling hydraulic fractures within mineral phases (LG-02, LG-06, LG-08, LG-12, LG-14, LG-15) (Figs. 2b and 3e-f; Table S2). Compositionally, these veins represent the quenching of strong alkaline melts ($Na_2O + K_2O$ = 7.37–9.59 wt%) characterized by high-K contents (2.84–4.37 wt%). They can be classified as high-SiO_2 (>60 %, HSA: SiO_2 > 60 wt%) and low-SiO_2 adakite (<51 %, LSA, SiO_2 < 60 wt%) glass (Martin et al., 2005) (Fig. S4). Due to their higher K_2O and TiO_2, as well as slightly lower Al_2O_3, CaO, and MgO at a given SiO_2 content, high-SiO_2 glass veins from Los Gemelos differ from the adakite lavas from Patagonia (Mahlburg Kay et al., 1993; Stern and Kilian, 1996; Ramos et al., 2004; Corgne et al., 2018), experimental studies (Rapp et al., 1999; Corgne et al., 2018), as well as from adakite glasses veins in metasomatized peridotites from Cerro del Fraile (Kilian and Stern, 2002) (Fig. S4). Regarding Na_2O, our samples overlap the samples mentioned above. This comparison can be extended to adakite glasses of metasomatized peridotites from the Avacha and Luzon arcs (Arai et al., 2003, 2004; Ishimaru et al., 2007) (Fig. S4). In contrast, the low-SiO_2 veins from Los Gemelos show strong affinity with low-SiO_2 adakite lavas from the East Coast rifted margin from the United States of America (Meyer and van Wijk, 2015) (Fig. S4). Independent of SiO_2 content, the Mg# of veins from Los Gemelos is high (0.56–0.64), which indicates

contribution of a peridotitic component.

Concerning the time of this metasomatic event, the lack of reaction zones in the peridotitic paragenesis associated with the glass veins, as well as the expectation that at mantle conditions they would be re-equilibrated with the surrounding peridotites during long lithospheric residence, we presume that the veins were formed by relatively recent/young processes, close to the time of eruption of the host basalt.

5.4. Implications for tectonic evolution of Patagonian lithosphere

Mantle xenoliths from Los Gemelos were transported to the surface during the Pleistocene (0.45 ± 0.03 Ma, Table S1). They record relatively high degrees of partial melting (16–28 %) that occurred during the Mesoproterozoic (1.3–0.9 Ga). Their Grenvillian ages can be associated to the formation and stabilization of the Patagonian SCLM that occurred during the Rodinia amalgamation. Pankhurst et al. (2014) reported U—Pb Grenvillian ages (1.1–0.9 Ga) for zircon cores from a biotite granite (VAL010) yielding Hf model ages between 1.4 and 1.3 Ga and juvenile εHf (+7.1 to +8.2). This confirms the depleted mantle source contribution to the initial formation of continental crust in this area. The *Re*—Os isotopic compositions and T_{RD} model ages obtained for Los Gemelos xenoliths (1.13–0.63 Ga) are similar to previous results obtained for mantle xenoliths from the Deseado Massif (T_{RD} ages = 1.34–0.50 Ga, n = 9) and the North Patagonian Massif (T_{RD} ages = 1.30–0.43 Ga, n = 23) (Schilling et al., 2008, 2017; Mundl et al., 2015, 2016). However, older ages also were reported for mantle xenoliths from the Deseado Massif (T_{RD} ages = 2.13–1.52 Ga, n = 8). Based on these Paleo- to Mesoproterozoic ages, Schilling et al. (2017) related the formation of the SCLM beneath the Deseado and North Patagonian massifs to the Malvinas/Falkland Islands and to the Namaqua-Natal province (southern South Africa) (e.g., Thomas et al., 2000; Wareham et al., 1998). Therefore, we conclude that the Los Gemelos peridotites provide additional evidence about the participation of Patagonia together with other continental blocks in the amalgamation of Rodinia supercontinent.

After crustal formation of Patagonia during the Proterozoic, different tectonic events may have been responsible to explain the modal and cryptic metasomatism shown by Los Gemelos peridotites. Considering that the generation of adakite melts requires high temperature (heat influx), these events are likely to involve the development of slab-windows and asthenospheric upwelling. Subduction of young and hot oceanic crust related to the Chile Ridge under South America resulted in the formation of adakitic lavas in the Austral Volcanic Zone during the Holocene (Stern and Kilian, 1996). Also, Miocene adakites are reported further east (average age of 12.50 ± 1.13 Ma; Ramos et al., 1991, 2004; Mahlburg Kay et al., 1993; Motoki et al., 2003). However, adakites were not described in the Southern Volcanic Zone (SVZ) or even in its back-arc region.

Mantle xenoliths from Cerro del Fraile brought to the surface by Pleistocene alkaline basalts (2.44–1.01 Ma, Fleck et al., 1972) are characterized by adakite metasomatism (Kilian and Stern, 2002; Faccini et al., 2013). These xenoliths are the closest to the Chile Trench (280 km), followed by Chile Chico (300 km) and Coyhaique (320 km). The subduction-related metasomatism recorded by mantle xenoliths from Coyhaique, SW of Los Gemelos, is a consequence of the opening of a Paleocene-Eocene slab-window related to the Farallon-Aluk ridge collision and subduction beneath Patagonia (Jalowitzki et al., 2017). We consider that the Paleocene-Eocene metasomatism recorded by mantle xenoliths from Los Gemelos, at a distance of ~600 km from the active margin, was possible due to the lithospheric thinning shown by low elastic thickness (T_e) values in the study area (Tassara et al., 2007; Schilling et al., 2017; Jalowitzki et al., 2024) (Fig. 10). This anomalous shallow lithosphere-asthenosphere boundary is identified at ~60 km depth (Priestley et al., 2019; Jalowitzki et al., 2024).

These results are corroborated by seismic tomographic data (SA2019, Celli et al., 2020), which reveals a strong low-velocity anomaly in the mantle wedge beneath Central-North Patagonia (~50–180 km). This anomaly possibly reflects thermal evidence of the connection between a ~ N-S slab tearing related to the Farallon-Aluk oceanic plate during the Paleocene-Eocene (north of 46°30′S) and the slab-window produced by the Miocene to Present collision of the Chile ridge (south of 46°30′S) (Zaffarana et al., 2019; Navarrete et al., 2021). Therefore, the low-velocity seismic anomaly located north of 46°S represents a compositional rather thermal anomaly beneath Canquel Plateau. Remarkably, the estimated time for the *rhenium*-enrichment (~60 Ma) of sample LG-01 coincides with the Paleocene-Eocene ridge subduction (Fig. 10).

6. Conclusion

Here we report new insights about the complex and long-lived SCLM evolution beneath the Patagonian back-arc by examining spinel-bearing mantle xenoliths from the Los Gemelos volcano, Canquel Plateau. They are mainly harzburgites with a few clinopyroxene-poor lherzolites characterized by high-degrees of melt extraction (16–28 %) with superimposed enrichment (metasomatism). The depleted character is evidenced by low whole-rock Al_2O_3 and CaO contents (both <1.5 wt%), high Mg# olivine (>90), and Cr-rich spinel (Cr# >0.20), together with correlations between Mg# vs. CaO, Al_2O_3, Na_2O, and TiO_2 in whole-rock

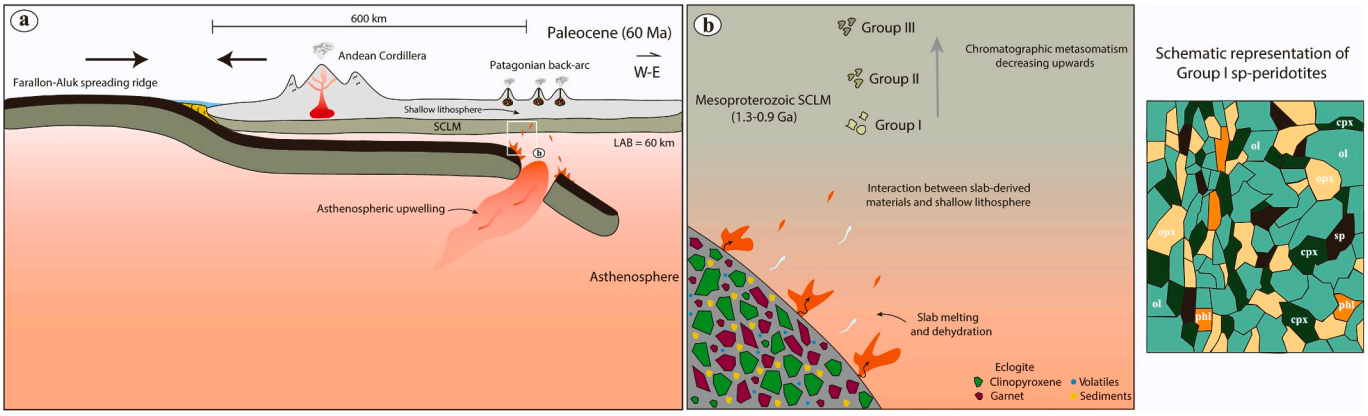

Fig. 10. Geodynamic model showing the development of a slab-window as a response to the subduction of the Farallon-Aluk ridge against the South America plate during the Paleocene (~60 Ma) (a). Mesoproterozoic (1.3–0.9 Ga) highly-depleted thin lithosphere (~60 km, Priestley et al., 2019; Jalowitzki et al., 2024) beneath Los Gemelos volcano was metasomatized by dehydration and partial melting of a hydrous eclogitized oceanic crust ~600 km far from the Andean Cordillera (a, b). The chromatographic metasomatism preferentially affecting the deeper lithosphere is illustrated in detail (b), where phlogopite-bearing mantle xenoliths from Group I are strongly metasomatized compared with the shallower Groups II and III.

and pyroxenes. In addition, HSE patterns support this assumption with relative depletions in the incompatible elements Re and Pd. Re—Os model ages and the positive correlations between $^{187}Os/^{188}Os$ vs. whole-rock Al_2O_3 (wt%) suggest that partial melting occurred during the Mesoproterozoic (1.3–0.9 Ga).

The petrographic and chemical characteristics of the SCLM beneath Los Gemelos reflect modal and cryptic metasomatism. Modal metasomatism is evidenced by phlogopite crystallization and by the cross-cutting networks of glass veins with alkaline composition containing low- and high-SiO_2. Also, cryptic metasomatism is evidenced by the selective enrichment of LREE (La—Ce) compared to the other REEs in clinopyroxene ($La/Pr_N = 1.50–6.89$), as well as by the U-shaped REE pattern shown by whole-rock compositions ($La/Sm_N > 1$ and $Gd/Yb_N < 1$). Major (i.e., Mg# vs. basaltic elements) and trace (i.e., La/Yb_N vs. Sr/Y and Ti/Eu; and Sr vs. Ti/Eu) elements of pyroxenes strongly suggest the role of a silicate melt with adakite composition as a likely candidate for the metasomatic agent responsible for variable enrichment of the SCLM beneath Los Gemelos. The calculated melts in equilibrium with clinopyroxenes reveal that the G1 samples (with coexisting phlogopite) were strongly metasomatized by an adakite melt, whereas G2 and G3 samples, showing evidence for a chromatographic enrichment style, were only slightly affected by this metasomatic event. Therefore, it is reasonable to conclude that phlogopite crystallization and cryptic metasomatism recorded by mantle xenoliths is ultimately a product of partial melting of subducted hot oceanic crust plus sediments that triggered adakite melts in the mantle wedge related to the development of a slab-window during the Paleocene to Eocene.

CRediT authorship contribution statement

Aline Alves dos Santos: Writing – original draft, Methodology, Investigation. **Tiago Jalowitzki:** Writing – review & editing, Writing – original draft, Supervision, Methodology, Investigation, Funding acquisition, Conceptualization. **Fernanda Gervasoni:** Writing – review & editing, Conceptualization. **Maurizio Mazzucchelli:** Writing – review & editing, Methodology. **Tommaso Giovanardi:** Writing – review & editing, Methodology. **Manuel Enrique Schilling:** Writing – review & editing, Methodology. **Maria Isabel Varas-Reus:** Writing – review & editing, Methodology. **Yuji Orihashi:** Writing – review & editing, Methodology, Investigation, Conceptualization. **Rodrigo Freitas Rodrigues:** Writing – review & editing. **Richard Walter Carlson:** Writing – review & editing, Methodology. **Georgina Marianela Rubiano Lorenzoni:** Writing – review & editing, Methodology. **Daiji Hirata:** Writing – review & editing, Conceptualization. **Gustavo Walter Bertotto:** Writing – review & editing.

Declaration of competing interest

The authors declare that they have no known competing financial interests or personal relationships that could have appeared to influence the work reported in this paper.

Data availability

Data will be made available on request.

Acknowledgments

We thank the financial support given by the Serrapilheira Institute research project [grant number Serra-1709-18152]. Aline Alves dos Santos thanks the Coordenação de Aperfeiçoamento de Pessoal de Nível Superior – Brasil (CAPES) [Finance Code 001] for the Master scholarship. MIVR acknowledges funding from the DFG project [VA1568/1-1]. This work was possible due to the permission and hospitality of Mr. Gerardo Fernández Muller, owner of Estancia El Riscoso. The field work was supported by Prof. Miguel Haller, Gabriela Massaferro, and Viviana Alric. We thank the two anonymous reviewers for their constructive comments and, in particular, Dr. Sonja Aulbach for handling the manuscript with such commitment and dedication.

Appendix A. Supplementary data

Supplementary data to this article can be found online at https://doi.org/10.1016/j.chemgeo.2024.122412.

References

Anselmi, G., Panza, J., Cortés, J., Ragona, D., Genini, A., 2004. Hoja Geológica 4569-II El Sombrero, Provincia del Chubut. Bol. Serv. Geológico Min. Argentino 271, 70 (in Spanish).

Arai, S., 1987. An estimation of the least depleted spinel on the basis of the olivine-spinel mantle array. Neues Jb. Mineral. Monat. 8, 347–354.

Arai, S., Ishimaru, S., 2008. Insights into Petrological Characteristics of the Lithosphere of Mantle Wedge beneath Arcs through Peridotite Xenoliths: a Review. J. Petrol. 49 (4), 665–695. https://doi.org/10.1093/petrology/egm069.

Arai, S., Ishimaru, S., Okrugin, V.M., 2003. Metasomatized harzburgite xenoliths from Avacha volcano as fragments of mantle wedge of the Kamchatka arc: an implication for the metasomatic agent. Island Arc 12, 233–246. https://doi.org/10.1046/j.1440-1738.2003.00392.x.

Arai, S., Takada, S., Michibayashi, K., Kida, M., 2004. Petrology of peridotite xenoliths from Iraya Volcano, Philippines, and its implication for dynamic mantle-wedge processes. J. Petrol. 45, 369–389. https://doi.org/10.1093/petrology/egg100.

Aulbach, S., Sun, J., Tappe, S., Höfer, H.E., Gerdes, A., 2017. Volatile-rich Metasomatism in the Cratonic Mantle beneath SW Greenland: link to Kimberlites and Mid-lithospheric Discontinuities. J. Petrol. 58 (12), 2311–2338. https://doi.org/10.1093/petrology/egy009.

Aulbach, S., Lin, A.-B., Weiss, Y., Yaxley, G.M., 2020. Wehrlites from continental mantle monitor the passage and degassing of carbonated melts. Geochem. Persp. Let. 15, 30–34. https://doi.org/10.7185/geochemlet.2031.

Becker, H., Horan, M.F., Walker, R.J., Gao, S., Lorand, J.-P., Rudnick, R.L., 2006. Highly siderophile element composition of the Earth's primitive upper mantle: Constraints from new data on peridotite massifs and xenoliths. Geochim. Cosmochim. Acta 70, 4528–4550. https://doi.org/10.1016/j.gca.2006.06.004.

Bertotto, G.W., Mazzucchelli, M., Zanetti, A., Vannucci, R., 2013. Petrology and geochemistry of the back-arc lithospheric mantle beneath eastern Payunia (La Pampa, Argentina): evidence from Agua Poca peridotite xenoliths. Geochem. J. 47, 219–234. https://doi.org/10.2343/geochemj.2.0256.

Bertotto, G.W., Mazzucchelli, M., Zanetti, Al, Ponce, A.D., Giovanardi, T., Brunelli, D., Bernardi, M.I., Hémond, C.H., Cipriani, A., 2021. Mantle heterogeneities produced by open-system melting and melt/rock reactions in Patagonian extra-Andean backarc mantle (Paso de Indios, Argentina). J. S. Am. Earth Sci. 106, 103002. https://doi.org/10.1016/j.jsames.2020.103002.

Bertotto, G.W., Mazzucchelli, M., Giovanardi, T., Conceição, R.V., Zanetti, A., Schilling, M.E., Bernardi, M.I., Ponce, A.D., Jalowitzki, T., Gervasoni, F., Cipriani, A., 2022. Mantle Xenoliths from Huanul Volcano (Central-West Argentina): a Poorly Depleted Mantle Source under Southern Payenia. Geosciences 12, 157. https://doi.org/10.3390/geosciences12040157.

Bjerg, E.A., Ntaflos, T., Kurat, G., Dobosi, G., Labudía, C.H., 2005. The upper mantle beneath Patagonia, Argentina, documented by xenoliths from alkali basalts. J. S. Am. Earth Sci. 18, 125–145. https://doi.org/10.1016/j.jsames.2004.09.002.

Bjerg, E.A., Ntaflos, T., Thöni, M., Aliani, P., Labudia, C.H., 2009. Heterogeneous lithospheric mantle beneath Northern Patagonia: evidence from Prahuaniyeu garnet- and spinel-peridotites. J. Petrol. 50, 1267–1298. https://doi.org/10.1093/petrology/egp021.

Bodinier, J.-L., Menzies, M.A., Shimizu, N., Frey, F.A., McPherson, E., 2004. Silicate, Hydrous and Carbonate Metasomatism at Lherz, France: Contemporaneous Derivatives of Silicate Melt-Harzburgite Reaction. J. Petrol. 45, 299–320. https://doi.org/10.1093/petrology/egg107.

Bonadiman, C., Brombin, V., Andreozzi, G.B., Benna, P., Coltorti, M., Curetti, N., Faccini, B., Merli, M., Pelorosso, B., Stagno, V., Tesauro, M., Pavese, A., 2021. Phlogopite-pargasite coexistence in an oxygen reduced spinel-peridotite ambient. Sci. Rep. 11, 11829. https://doi.org/10.1038/s41598-021-90844-w.

Braga, L.G., Jalowitzki, T., Gervasoni, F., Rodrigues, R.F., Mazzucchelli, M., Giovanardi, T., Dalla Costa, M.M., Santos, R.V., Rocha, M.P., Fuck, R.A., Lorenzoni, G.R., Bertotto, G.W., 2024. Destruction of the Lithosphere beneath the SW margin of the São Francisco Craton Evidenced by Refertilized and Deformed Mantle Xenoliths. J. Petrol. 65, egae087. https://doi.org/10.1093/petrology/egae087.

Breitsprecher, K., Thorkelson, D.J., 2009. Neogene kinematic history of Nazca Antarctic-Phoenix slab windows beneath Patagonia and the Antarctic Peninsula. Tectonophysics 464, 10–20. https://doi.org/10.1016/j.tecto.2008.02.013.

Brey, G.P., Köhler, T., 1990. Geothermobarometry in four-phase lherzolites II. New thermobarometers, and practical assessment of existing thermobarometers. J. Petrol. 31 (6), 1353–1378. https://doi.org/10.1093/petrology/31.6.1313.

Cande, S.C., Leslie, R.B., 1986. Late Cenozoic tectonics of the Southern Chile Trench. J. Geophys. Res. Solid Earth 91, 471. https://doi.org/10.1029/JB091iB01p00471.

Canil, D., Scarfe, C.M., 1989. Origin of Phlogopite in Mantle Xenoliths from Kostal Lake, Wells Gray Park, British Columbia. J. Petrol. 30 (5), 1159–1179. https://doi.org/10.1093/petrology/30.5.1159.

Castillo, P.R., 2012. Adakite petrogenesis. Lithos 134–135, 304–316. https://doi.org/10.1016/j.lithos.2011.09.013.
Celli, N.L., Lebedev, S., Schaeffer, A.J., Ravenna, M., Gaina, C., 2020. The upper mantle beneath the South Atlantic Ocean, South America and Africa from waveform tomography with massive data sets. Geophys. J. Int. 221, 178–204. https://doi.org/10.1093/gji/ggz574.
Corgne, A., Schilling, M.E., Grégoire, M., Langlade, J., 2018. Experimental constraints on metasomatism of mantle wedge peridotites by hybridized adakitic melts. Lithos 308–309, 213–226. https://doi.org/10.1016/j.lithos.2018.03.006.
Dantas, C., Grégoire, M., Koester, E., Conceição, R.V., Rieck, N., 2009. The lherzolite–websterite xenolith suite from Northern Patagonia (Argentina): evidence of mantle–melt reaction processes. Lithos 107, 107–120. https://doi.org/10.1016/j.lithos.2008.06.012.
Defant, M.J., Drummond, M.S., 1990. Derivation of some modern arc magmas by melting of young subducted lithosphere. Nature 347, 662–665. https://doi.org/10.1038/347662a0.
Dick, H.J.B., Fisher, R.L., 1984. Mineralogic studies of the residues of mantle melting: Abyssal and alpine type peridotites. Dev. Petrol. 11 (2), 295–308. https://doi.org/10.1016/B978-0-444-42274-3.50031-7.
D'Orazio, M., Innocenti, F., Manetti, P., Tamponi, M., Tonarini, S., González-Ferrán, O., Lahsen, A., Omarini, R., 2003. The Quaternary calc-alkaline volcanism of the Patagonian Andes close to the Chile triple junction: geochemistry and petrogenesis of volcanic rocks from the Cay and Maca volcanoes (~45°S, Chile). J. S. Am. Earth Sci. 16, 219–242. https://doi.org/10.1016/S0895-9811(03)00063-4.
Faccini, B., Bonadiman, C., Coltorti, M., Grégoire, M., Siena, F., 2013. Oceanic Material Recycled within the Sub-Patagonian Lithospheric Mantle (Cerro del Fraile, Argentina). J. Petrol. 54, 1211–1258. https://doi.org/10.1093/petrology/egt010.
Fallon, T.J., Danyushevsky, L.V., Crawford, A.J., Meffre, S., Woodhead, J.D., Bloomer, S. H., 2008. Boninites and Adakites from the Northern termination of the Tonga Trench: Implications for Adakite Petrogenesis. J. Petrol. 49 (4), 697–715. https://doi.org/10.1093/petrology/egm080.
Fleck, R., Mercer, J., Nairn, A., Peterson, D., 1972. Chronology of late Pliocene and early Pleistocene glacial and magnetic events in southern Argentina. Earth Planet. Sci. Lett. 16, 15–22. https://doi.org/10.1016/0012-821X(72)90231-2.
Franz, L., Becker, K.-P., Kramer, W., Herzig, P.M., 2002. Metasomatic mantle xenoliths from the Bismarck microplate (Papua New Guinea) — thermal evolution, geochemistry and extent of slab-induced metasomatism. J. Petrol. 43 (2), 315–343. https://doi.org/10.1093/petrology/43.2.315.
Gervasoni, F., Klemme, S., Rohrbach, A., Grützner, T., Berndt, J., 2017. Experimental constraints on mantle metasomatism caused by silicate and carbonate melts. Lithos 282–283, 173–186. https://doi.org/10.1016/j.lithos.2017.03.004.
Gervasoni, F., Jalowitzki, T., Rocha, M.P., Weska, R.K., Novais-Rodrigues, E., Rodrigues, R.A.F., Bussweiler, Y., Barbosa, E.S.R., Berndt, J., Dantas, E.L., Souza, V. S., Klemme, S., 2022. Recycling process and proto-kimberlite melt metasomatism in the lithosphere-asthenosphere boundary beneath the Amazonian Craton recorded by garnet xenocrysts and mantle xenoliths from the Carolina kimberlite. Geosci. Front. 13, 101429. https://doi.org/10.1016/j.gsf.2022.101429.
Giuliani, A., Phillips, D., Kamenetsky, V.S., Kendrick, M.A., Wyatt, B.A., Goemann, K., Hutchinson, G., 2014. Petrogenesis of mantle polymict breccias: insights into mantle processes coeval with kimberlite magmatism. J. Petrol. 55, 831–858. https://doi.org/10.1093/petrology/egu008.
Giuliani, A., Phillips, D., Kamenetsky, V.S., Goemann, K., 2016. Constraints on kimberlite ascent mechanisms revealed by phlogopite compositions in kimberlites and mantle xenoliths. Lithos 240–243, 189–201. https://doi.org/10.1016/j.lithos.2015.11.013.
Gorring, M.L., Kay, S.M., 2000. Carbonatite metasomatized peridotite xenoliths from southern Patagonia: Implications for lithospheric processes and Neogene plateau magmatism. Contrib. Mineral. Petrol. 140, 55–72. https://doi.org/10.1007/s004100000164.
Grégoire, M., McInnes, B.I.A., O'Reilly, S.Y., 2001. Hydrous metasomatism of oceanic sub-arc mantle, Lihir, Papua New Guinea Part 2. Trace element characteristics of slab-derived fluids. Lithos 59, 91–108. https://doi.org/10.1016/S0024-4937(01)00058-5.
Grégoire, M., Bell, D.R., Le Roex, A.P., 2002. Trace element geochemistry of phlogopite-rich mafic mantle xenoliths: their classification and their relationship to phlogopite-bearing peridotites and kimberlites revisited. Contrib. Mineral. Petrol. 142, 603–625. https://doi.org/10.1007/s00410-001-0315-8.
Hervé, F., Fanning, C.M., Pankhurst, R.J., 2003. Detrital zircon age patterns and provenance of the metamorphic complexes of southern Chile. J. S. Am. Earth Sci. 16, 107–123. https://doi.org/10.1016/S0895-9811(03)00022-1.
Ionov, D.A., Bodinier, J.-L., Mukasa, S.B., Zanetti, A., 2002. Mechanisms and sources of Mantle Metasomatism: Major and Trace Element Compositions of Peridotite Xenoliths from Spitsbergen in the Context of Numerical Modelling. J. Petrol. 43 (12), 2219–2259. https://doi.org/10.1093/petrology/43.12.2219.
Ishimaru, S., Arai, S., Ishida, Y., Shirasaka, M., Okrugin, V.M., 2007. Melting and Multi-stage Metasomatism in the Mantle Wedge beneath a Frontal Arc Inferred from Highly Depleted Peridotite Xenoliths from the Avacha Volcano, Southern Kamchatka. J. Petrol. 48 (2), 395–433. https://doi.org/10.1093/petrology/egl065.
Jalowitzki, T., Sumino, H., Conceição, R.V., Orihashi, Y., Nagao, K., Bertotto, G.W., Balbinot, E., Schilling, M.E., Gervasoni, F., 2016. Noble gas composition of subcontinental lithospheric mantle: an extensively degassed reservoir beneath Southern Patagonia. Earth Planet. Sci. Lett. 450, 263–273. https://doi.org/10.1016/j.epsl.2016.06.034.
Jalowitzki, T., Gervasoni, F., Conceição, R.V., Orihashi, Y., Bertotto, G.W., Sumino, H., Schilling, M.E., Nagao, K., Morata, D., Sylvester, P., 2017. Slab-derived components in the subcontinental lithospheric mantle beneath Chilean Patagonia: Geochemistry and Sr–Nd–Pb isotopes of mantle xenoliths and host basalt. Lithos 292–293, 179–197. https://doi.org/10.1016/j.lithos.2017.09.008.
Jalowitzki, T., Sumino, H., Conceição, R.V., Schilling, M.E., Bertotto, G.W., Tassara, A., Gervasoni, F., Orihashi, Y., Nagao, K., Rocha, M.P., Rodrigues, R.A.F., 2024. Pristine helium from the Karoo mantle plume within the shallow asthenosphere beneath Patagonia. Nat. Commun. 15, 6402. https://doi.org/10.1038/s41467-024-50773-4.
Jochum, K., Nohl, U., Herwig, K., Lammel, E., Stoll, B., Hofmann, A.W., 2005. GeoReM: a New Geochemical Database for Reference Materials and Isotopic Standards. Geostand. Geoanal. Res. 29 (3), 333–338. https://doi.org/10.1111/j.1751-908X.2005.tb00904.x.
Jochum, K.P., Weis, U., Schwager, B., Stoll, B., Wilson, S.A., Haug, G.H., Meinrat, A.O., Enzweiler, J., 2015. Reference values following ISO guidelines for frequently requested rock reference materials: Geostand. Geoanalytical Res. 40, 333–350. https://doi.org/10.1111/j.1751-908X.2015.00392.x.
Kargin, A.V., Sazonova, L.V., Nosova, A.A., Lebedeva, N.M., Kostitsyn, Yu.A., Kovalchuk, E.V., Tretyachenko, V.V., Tikhomirova., Y. A.S., 2019. Phlogopite in mantle xenoliths and kimberlite from the Grib pipe, Arkhangelsk province, Russia: evidence for multi-stage mantle metasomatism and origin of phlogopite in kimberlite. Geosci. Front. 10, 1941–1959. doi:https://doi.org/10.1016/j.gsf.2018.12.006.
Kepezhinskas, P., Defant, M.J., 2001. Nonchondritic Pt/Pd ratios in arc mantle xenoliths: evidence for platinum enrichment in depleted island-arc mantle sources. Geology 29 (9), 851–854. https://doi.org/10.1130/0091-7613(2001)029<0851:NPPRIA>2.0.CO;2.
Kepezhinskas, P.K., Defant, M.J., Drummond, M.S., 1995. Na Metasomatism in the Island-Arc Mantle by Slab Melt-Peridotite Interaction: evidence from Mantle Xenoliths in the North Kamchatka Arc. J. Petrol. 36 (6), 1505–1527. https://doi.org/10.1093/oxfordjournals.petrology.a037263.
Kilian, R., Behrmann, J.H., 2003. Geochemical constraints on the sources of Southern Chile Trench sediments and their recycling in arc magmas of the Southern Andes. J. Geol. Soc. Lond. 160, 57–70. https://doi.org/10.1144/0016-764901-143.
Kilian, R., Stern, C.R., 2002. Constraints on the interaction between slab melts and the mantle wedge from adakitic glass in peridotite xenoliths. Eur. J. Mineral. 14, 25–36. https://doi.org/10.1127/0935-1221/2002/0014-0025.
Laurora, A., Mazzucchelli, M., Rivalenti, G., Vannucci, R., Zanetti, A., Barbieri, M.A., Cingolani, C.A., 2001. Metasomatism and Melting in Carbonated Peridotite Xenoliths from the Mantle Wedge: the Gobernador Gregores Case (Southern Patagonia). J. Petrol. 42, 69–87. https://doi.org/10.1093/petrology/42.1.69.
Luguet, A., Nowell, G.M., Pearson, D.G., 2008. $^{184}Os/^{188}Os$ and $^{186}Os/^{188}Os$ measurements by negative thermal Ionisation Mass Spectrometry (N-TIMS): Effects of interfering element and mass fractionation corrections on data accuracy and precision. Chem. Geol. 248, 342–362. https://doi.org/10.1016/j.chemgeo.2007.10.013.
Mahlburg Kay, S., Ramos, V., Marquez, M., 1993. Evidence in Cerro Pampa Volcanic Rocks for Slab-Melting prior to Ridge-Trench Collision in Southern South America. J. Geol. 101, 703–714. https://doi.org/10.1086/648269.
Martin, H., Smithies, R.H., Rapp, R., Moyen, J.F., Champion, D., 2005. An overview of adakite, tonalite–trondhjemite–granodiorite (TTG), and sanukitoid: relationships and some implications for crustal evolution. Lithos 79, 1–24. https://doi.org/10.1016/j.lithos.2004.04.048.
Martínez Dopico, C.I., López de Luchi, M.G., Rapalini, A.E., Kleinhanns, I.C., 2011. Crustal segments in the North Patagonian Massif, Patagonia: an integrated perspective based on Sm–Nd isotope systematics. J. S. Am. Earth Sci. 31 (2–3), 324–341. https://doi.org/10.1016/j.jsames.2010.07.009.
Massaferro, G.I., Orihashi, Y., Alric, V., Jalowitzki, T., Hirata, D., 2017. Características químicas de elementos mayores y trazas de la Formación Sierra Cuadrada en la Meseta del Canquel, Chubut, in: XX Congreso Geológico Argentino. San Miguel de Tucumán, Argentina, pp. 69–74 (In Spanish).
Meisel, T., Walker, R.J., Irving, A.J., Lorand, J.-P., 2001. Osmium isotopic compositions of mantle xenoliths: a global perspective. Geochim. Cosmochim. Acta 65, 1311–1323. https://doi.org/10.1016/S0016-7037(00)00566-4.
Melchiorre, M., Faccini, B., Grégoire, M., Benoit, M., Casetta, F., Coltorti, M., 2020. Melting and metasomatism/refertilisation processes in the Patagonian sub-continental lithospheric mantle: a review. Lithos 354–355, 1–16. https://doi.org/10.1016/j.lithos.2019.105324.
Mercier, J.C.C., Nicolas, A., 1975. Textures and fabrics of upper-mantle peridotites as illustrated by xenoliths from basalts. J. Petrol. 16, 454–487. https://doi.org/10.1093/petrology/16.1.454.
Meyer, R., van Wijk, J., 2015. Post-breakup lithosphere recycling below the U.S. East Coast: Evidence from adakitic rocks. In: Foulger, G.R., Lustrino, M., King, S.D. (Eds.), The Interdisciplinary Earth: A Volume in Honor of Don L. Anderson: Geological Society of America Special Paper 514 and American Geophysical Union Special Publication 71, pp. 65–85. https://doi.org/10.1130/2015.2514(06.
Motoki, A., Orihashi, Y., Hirata, D., Haller, M.J., Ramos, V.A., Schilling, M., Iwano, H., Cario, F.D., Anma, R., 2003. U–Pb dating for single grain zircon using laser ablation ICP mass spectrometer and fission track ages of zircon for back-arc adakitic bodies, the Cerro Pampa and the Puesto Nuevo, argentine Patagonia. Short Papers of VI South American Symposium on Isotopic Geology 1, 108–110.
Mundl, A., Ntaflos, T., Ackerman, L., Bizimis, M., Bjerg, E.A., Hauzenberger, C.A., 2015. Mesoproterozoic and Paleoproterozoic subcontinental lithospheric mantle domains beneath southern Patagonia: isotopic evidence for its connection to Africa and Antarctica. Geology 43, 39–42. https://doi.org/10.1130/G36344.1.
Mundl, A., Ntaflos, T., Ackerman, L., Bizimis, M., Bjerg, E.A., Wegner, W., Hauzenberger, C.A., 2016. Geochemical and Os–Hf–Nd–Sr isotopic characterization of North Patagonian Mantle Xenoliths: implications for extensive melt extraction and percolation processes. J. Petrol. 57, 685–715. https://doi.org/10.1093/petrology/egv048.

Navarrete, C.R., Massaferro, G., Gianni, G.A., Lastra, M.B., 2021. The slab gap-related late Cretaceous-Paleocene magmatism of southern Patagonia. J. Geodyn. 147, 101869. https://doi.org/10.1016/j.jog.2021.101869.
Neumann, E.-R., Wulff-Pedersen, E., 1997. The Origin of Highly Silicic Glass in Mantle Xenoliths from the Canary Islands. J. Petrol. 38 (11), 1513–1539. https://doi.org/10.1093/petroj/38.11.1513.
Neumann, E.-R., Griffin, W.L., Pearson, N.J., O'reilly, S.Y., 2004. The Evolution of the Upper Mantle beneath the Canary Islands: Information from Trace elements and Sr isotope Ratios in Minerals in Mantle Xenoliths. J. Petrol. 45 (12), 2573–2612. https://doi.org/10.1093/petrology/egh063.
Nimis, P., Grütter, H., 2010. Internally consistent geothermometers for garnet peridotites and pyroxenites. Contrib. Mineral. Petrol. 159, 411–427. https://doi.org/10.1007/s00410-009-0455-9.
Novais-Rodrigues, E., Jalowitzki, T., Gervasoni, F., Sumino, H., Bussweiler, Y., Klemme, S., Berndt, J., Conceição, R.V., Schilling, M.E., Bertotto, G.W., Teles, L., 2021. Partial melting and subduction-related metasomatism recorded by geochemical and isotope (He-Ne-Ar-Sr-Nd) compositions of spinel lherzolite xenoliths from Coyhaique, Chilean Patagonia. Gondwana Res. 98, 257–276. https://doi.org/10.1016/j.gr.2021.06.003.
Ntaflos, T., Bjerg, E.A., Labudia, C.H., Kurat, G., 2007. Depleted lithosphere from the mantle wedge beneath Tres Lagos, southern Patagonia, Argentina. Lithos 94, 46–65. https://doi.org/10.1016/j.lithos.2006.06.011.
Pankhurst, R.J., Rapela, C.R., 1995. Production of Jurassic rhyolite by anatexis of the lower crust of Patagonia. Earth Planet. Sci. Lett. 134, 23–36. https://doi.org/10.1016/0012-821X(95)00103-J.
Pankhurst, R.J., Rapela, C.W., Loske, W.P., Márquez, M., Fanning, C.M., 2003. Chronological study of the pre-Permian basement rocks of southern Patagonia. J. S. Am. Earth Sci. 16, 27–44. https://doi.org/10.1016/S0895-9811(03)00017-8.
Pankhurst, R.J., Rapela, C.W., Fanning, C.M., Márquez, M., 2006. Gondwanide continental collision and the origin of Patagonia. Earth-Science Rev. 76, 235–257. https://doi.org/10.1016/j.earscirev.2006.02.001.
Pankhurst, R.J., Rapela, C.W., López de Luchi, M.G., Rapalini, A.E., Fanning, C.M., Galindo, C., 2014. The Gondwana connections of northern Patagonia. J. Geol. Soc. Lond. 171, 313–328. https://doi.org/10.1144/jgs2013-081.
Pearson, D.G., Irvine, G.J., Ionov, D.A., Boyd, F.R., Dreibus, G.E., 2004. Re–Os isotope systematics and platinum group element fractionation during mantle melt extraction: a study of massif and xenolith peridotite suites. Chem. Geol. 208, 29–59. https://doi.org/10.1016/j.chemgeo.2004.04.005.
Priestley, K., McKenzie, D., Ho, T.A., 2019. Lithosphere–Asthenosphere Boundary– A Global Model Derived from Multimode Surface-Wave Tomography and Petrology. Lithospheric Discontinuities, Geophysical Monograph 239, Chapter 6, First edition. Edited by Huaiyu Yuan and Barbara Romanowicz. American Geophysical Union. Published by John Wiley & Sons, Inc.
Ramos, V.A., 2010. The Grenville-age basement of the Andes. J. S. Am. Earth Sci. 29, 77–91. https://doi.org/10.1016/j.jsames.2009.09.004.
Ramos, V.A., Kay, S.M. y Márquez, M. 1991. La Dacita Cerro Pampa (Mioceno - provincia de Santa Cruz): evidencias de la colision de una dorsal oceánica. VI° Congreso Geológico Chileno (Viña del Mar) Actas I: 747–751 (In Spanhish).
Ramos, V.A., Kay, S.M., Singer, B.S., 2004. Las adakitas de la Cordillera Patagónica: Nuevas evidencias geoquímicas y geocronológicas. Rev. Asoc. Geol. Argent. 59 (4), 693–706.
Rampone, E., Bottazzi, P., Ottolini, L., 1991. Complementary Ti–Zr anomalies in orthopyroxene and clinopyroxene in mantle peridotites. Nature 354, 518–520. https://doi.org/10.1038/354518a0.
Rapp, R.P., Shimizu, N., Norman, M.D., Applegate, G.S., 1999. Reaction between slab-derived melts and peridotite in the mantle wedge: experimental constraints at 3.8 GPa. Chem. Geol. 160, 335–356. https://doi.org/10.1016/S0009-2541(99)00106-0.
Reisberg, L., Meisel, T., 2002. The Re-Os isotopic system: a review of analytical techniques. Geostand. Geoanal. Res. 26, 249–267. https://doi.org/10.1111/j.1751-908X.2002.tb00633.x.
Rivalenti, G., Zanetti, A., Mazzucchelli, M., Vannucci, R., Cingolani, C.A., 2004. Equivocal carbonatite markers in the mantle xenoliths of the Patagonia backarc: the Gobernador Gregores case (Santa Cruz Province, Argentina). Contrib. Mineral. Petrol. 147, 647–670. https://doi.org/10.1007/s00410-004-0582-2.
Rivalenti, G., Mazzucchelli, M., Zanetti, A., Vannucci, R., Bollinger, C., Hémond, C., Bertotto, G.W., 2007. Xenoliths from Cerro de los Chenques (Patagonia): an example of slab-related metasomatism in the backarc lithospheric mantle. Lithos 99, 45–67. https://doi.org/10.1016/j.lithos.2007.05.012.
Rodrigues, R.A.F., Gervasoni, F., Jalowitzki, T., Bussweiler, Y., Berndt, J., Botelho, N.F., Queiroga, G., Castro, M.P., Silva, S.W., Ciriaco, B.A., Oliveira, I.L., Klemme, S., 2023. Mantle metasomatism and refertilization beneath the SW margin of the São Francisco Craton, Brazil. Lithos 448–449, 107164. https://doi.org/10.1016/j.lithos.2023.107164.
Roduit, N., 2007. JMicroVision: un logiciel d'analyse d'images p trographiques polyvalent. PhD thesis. University of Genève, Switzerland, p. 116. https://doi.org/10.13097/archive-ouverte/unige:468 (In French).
Schilling, M.E., Carlson, R.W., Conceição, R.V., Dantas, C., Bertotto, G.W., Koester, E., 2008. Re–Os isotope constraints on subcontinental lithospheric mantle evolution of southern South America. Earth Planet. Sci. Lett. 268, 89–101. https://doi.org/10.1016/j.epsl.2008.01.005.
Schilling, M.E., Carlson, R.W., Tassara, A., Conceição, R.V., Bertotto, G.W., Vasquez, M., Munoz, D., Jalowitzki, T., Gervasoni, F., Morata, D., 2017. The origin of Patagonia revealed by Re-Os systematics of mantle xenoliths. Precambrian Res. 294, 15–32. https://doi.org/10.1016/j.precamres.2017.03.008.
Shirey, S.B., Walker, R.J., 1995. Carius tube digestion for low-blank rhenium-osmium analysis. Anal. Chem. 67, 2136–2141. https://doi.org/10.1021/ac00109a036.
Stachel, T., 2022. PTEXL - Geothermobarometry of Mantle Rocks. Borealis V2. https://doi.org/10.5683/SP3/IMYNCL.
Stern, C.R., Kilian, R., 1996. Role of the subducted slab, mantle wedge and continental crust in the generation of adakites from the Andean Austral Volcanic Zone. Contrib. Mineral. Petrol. 123, 263–281. https://doi.org/10.1007/s004100050155.
Stern, C.R., Kilian, R., Olker, B., Hauri, E.H., Kurtis Kyser, T., 1999. Evidence from mantle xenoliths for relatively thin (<100 km) continental lithosphere below the Phanerozoic crust of southernmost South America. Lithos 48 (1–4), 217–235. https://doi.org/10.1016/S0024-4937(99)00030-4.
Streckeisen, A., 1976. To each plutonic rock its proper name. Earth-Science Rev. 12, 1–33. https://doi.org/10.1016/0012-8252(76)90052-0.
Sun, S.-S., McDonough, W.F., 1989. Chemical and isotopic systematics of oceanic basalts: implications for mantle composition and processes. J. Geol. Soc. London Special Publication 42, 313–345. https://doi.org/10.1144/GSL.SP.1989.042.01.19.
Tappe, S., Smart, K., Torsvik, T., Massuyeau, M., de Wit, M., 2018. Geodynamics of kimberlites on a cooling Earth: Clues to plate tectonic evolution and deep volatile cycles. Earth Planet. Sci. Lett. 484, 1–14. https://doi.org/10.1016/j.epsl.2017.12.013.
Tassara, A., Swain, C., Hackney, R., Kirby, J., 2007. Elastic thickness structure of South America estimated using wavelets and satellite-derived gravity data. Earth Planet. Sci. Lett. 253, 17–36. https://doi.org/10.1016/j.epsl.2006.10.008.
Taylor, W.R., 1998. An experimental test of some geothermometer and geobarometer formulations for upper mantle peridotites with application to the thermobarometry of fertile lherzolite and garnet websterite. Neues Jahrbuch fur Mineralogie, Abhandlungen 172, 381–408.
Taylor, S.R., McLennan, S.M., 1985. The Continental Crust: Its Composition and Evolution. Blackwell, Oxford, UK.
Thomas, R.J., Jacobs, J., Eglington, B.M., 2000. Geochemistry and isotopic evolution of the Mesoproterozoic Cape Meredith complex, West Falkland. Geol. Mag. 137, 537–553. https://doi.org/10.1017/S0016756800004519.
Walker, R.J., Carlson, R.W., Shirey, S.B., Boyd, F.R., 1989. Os, Sr, Nd, and Pb isotope systematics of southern African peridotite xenoliths: Implications for the chemical evolution of subcontinental mantle. Geochim. Cosmochim. Acta 53, 1583–1595. https://doi.org/10.1016/0016-7037(89)90240-8.
Wareham, C.D., Pankhurst, R.J., Thomas, R.J., Storey, B.C., Grantham, G.H., Jacobs, J., Eglington, B.M., 1998. Pb, Nd, and Sr isotope mapping of Grenville-age crustal provinces in Rodinia. J. Geol. 106, 647–660. https://doi.org/10.1086/516051.
Wyllie, P.J., Sekine, T., 1982. The formation of mantle phlogopite in subduction zone hybridization. Contrib. Mineral. Petrol. 79 (4), 375–380. https://doi.org/10.1007/BF01132067.
Yaxley, G.M., Kamenetsky, V., Green, D.H., Falloon, T.J., 1997. Glasses in mantle xenoliths from western Victoria, Australia, and their relevance to mantle processes. Earth Planet. Sci. Lett. 148, 433–446. https://doi.org/10.1016/S0012-821X(97)00058-7.
Zaffarana, C., Lagorio, S., Orts, D., Busteros, A., Nieto, D.S., Giacosa, R., González, V.R., Boltshauser, B., Negre, C.P., Somoza, R., Haller, M., 2019. First geochemical and geochronological characterization of late cretaceous mesosilicic magmatism in Gastre, Northern Patagonia, and its tectonic relation to other coeval volcanic rocks in the region. Geol. Mag. 156, 1285–1294. https://doi.org/10.1017/S0016756818000432.